Artificial Cytoplasm: Observing Anomalous Diffusion & Progress Towards Drift-Reduction

Elisabeth Lawrence

May 4, 2023

Faculty Advisor: Viva Horowitz

Hamilton College

Department of Physics

Submitted as a Partial Requirement for the Senior Project

1 Abstract

The development of an artificial cell is desired to contribute to the understanding of biological intracellular environments. The goal of this work is to contribute to the artificial cells project by both determining the feasibility of an easily reproducible drift-reducing chamber and evaluating the replication of intracellular crowdedness using aqueous solutions including two polymer chain lengths of polyethylene glycol. The first part of this study focused on the creation of a drift-reducing chamber using agarose hydrogels. Despite the optimization of the chamber, in relation to agarose hydrogel specifications and construction methods, it was found to be unsuitable due to its inability to maintain a seal when fluid was flowed through the system. The second section of this work studied the motion of inert tracer particles in aqueous solutions with varying concentrations (16.7 mg/mL, 25 mg/mL, and a mixture of 40% concentration and 20 mg/mL) of two polyethylene glycol polymer chain lengths (2000 & 8000 or 200 & 20000). The related findings suggest both the diffusion coefficient A and the diffusive exponent α to depend on a medium's crowdedness and variation of particle sizes. Anomalous subdiffusion was observed in samples with a concentration of 25 mg/mL or above. This finding experimentally supports the theoretical work of Sunol and Zia [1] and aligns with the use of PEG for artificial replication of the crowdedness of biological cytoplasm. The tracer particle findings of this study have exciting implications for the artificial cells project and general work towards the creation of an artificial cell.

Contents

2 Acknowledgements

I offer my sincerest gratitude to my thesis advisor Professor Viva Horowitz. Her extensive work in the field prior to my involvement provided me with a wonderful project to join. Her unwavering support and continued enthusiasm throughout my thesis journey not only propelled my research forward but made the process fun. My contributions to this project would not have been possible without her help.

I would also like to thank additional professors, past and present, of the Hamilton College physics department who were particularly influential during my physics education at Hamilton College: Professor Kristen Burson, Professor Brian Collett, and my faculty advisor Professor Seth Major.

I am additionally extremely thankful for the help of Walter Zarnoch and Thomas Freeland in the machine shop. Their continued aid in making parts was necessary for the completion of this project.

I am incredibly grateful to my classmates and friends in the physics department who I have spent much time in class and working on problem sets with, particularly Elizabeth (Pippi) Seider and Clare Nelle. I would not be where I am today without their continued words of encouragement and, of course, fun study sessions.

Finally, I would like to acknowledge the many additional individuals in my personal life that have supported me through my undergraduate career at Hamilton College: my parents and siblings for their unconditional love and support, and my incredible friends outside of the department who despite their lack of shared academic interests and understanding of physics encouraged me every step of the way and always expressed their pride in my accomplishments. I can not thank them enough.

3 Introduction

3.1 Background

A biological cell's cytoplasm is a complex domain consisting of crowded organelles, organic molecules, salts, and water. Cytoplasm's spatial organization plays a massive role in biological systems– impacting cytokinesis, the movement of proteins, and many other integral processes [2]. Yet, while the complicated non-Newtonian properties of cytoplasm are documented, the underlying physical-chemical properties of cytoplasm are not well understood [3]. This knowledge gap calls for the development of artificial model systems of cells.

3.1.1 Intracellular Movement

Movement within intracellular environments can be generally categorized as one of two types: passive diffusion and active transport. Passive diffusion, also known as Brownian motion, is the random movement of particles in a fluid as a result of continuous bombardment from surrounding molecules. The theory of Brownian motion originates from the works of Einstein, Langevin, Smoluchowski, Fokker, and Plank [4] and will be discussed further in the Theory section of this paper. Active transport describes the energetically-driven movement of other molecules in the cytoplasm, including by the motion of motor proteins. These motors not only directly transport their cargo, but they can bolster the transport of unattached particles within the cytoplasm [5]. Studying the various types of intracellular movement works to further the understanding of cellular environments and biological processes.

Numerous studies have been conducted to observe the passive diffusion of particles in both artificially made and biological environments. In 1988, van Megen and Underwood experimentally studied the passive diffusion of tracer particles in colloidal suspensions [6]. At the same time, Kehr et al. (1989) investigated the interdiffusion of two species of particles, of different transition rates, in lattice-gas models [7]. Later on, Leptos et al. studied passive tracers, this time in a biological environment of suspensions of eukaryotic swimmers. Their work focused on the collective behavior generated by bacterial systems with high swimmer concentrations and the subsequent enhancement of tracer particle transport and fluid mixing [8]. Each of these studies worked to advance knowledge of passive diffusion.

The study of active transport is similarly extensive and encapsulates a vast variety of methods. Howse

et al. (2007) studied the motion of artificial micro-scale swimmers that use a chemical reaction catalyzed on their surfaces to achieve autonomous propulsion [9]. This experimental work helped solidify the ability to take advantage of chemical reactions to create effective autonomous propulsion of spherical colloids that mimic active transport within the cytoplasm. Previous work on this project has involved the study of active Pt-coated Janus particles which similarly make use of a chemical reaction by catalyzing the breakdown of hydrogen peroxide on their platinum-coated hemisphere to propel them forward and create concentration-field gradients [5]. The catalytic nature of these Janus particles allows them to use a surrounding medium, aqueous hydrogen peroxide, as a fuel reservoir while maintaining the integrity of the colloid:

$$2H_2O_2 \rightarrow^{Pt} 2H_2O + O_2. \tag{1}$$

These artificial chemical swimmers were studied alongside passive fluorescently dyed sulfate latex tracer particles (Fluoromax, 1.1 μm diameter) confined to emulsion droplets. The motion of both particles in fuel was tracked to better understand the coupling of active and passive particle motion [5].

More recently, thesis student Ryan Smolarsky focused his work on better replicating the crowdedness of biological cytoplasm by introducing various concentrations and polymer chain lengths of polyethylene glycol (PEG), Fig. 1, to sealed sample slides with RO water and tracer particles. Smolarsky observed the tracer particle diffusion in solutions with PEG lengths of 200, 2000, 8000, and 20000, each at approximately 3.3, 6.7, 10, 13.3, and 16.7 mg/mL concentration. Two primary variables were examined in this study: diffusion coefficient and diffusive exponent, both of which will be further explored in section 4. Data from these slides showed a decrease in diffusion coefficient with an increased PEG concentration or polymer chain length. Additionally, all measured diffusive exponents were shown to remain constant at $\alpha = 1$, which is consistent with basic passive diffusion [10]. While the diffusive exponent of $\alpha = 1$ is easily distinguishable from active transport, $\alpha = 2$, it is not fully representative of the anomalous motion that exists within biological cytoplasm as a result of their crowdedness.

Published March 2023, theoretical work by Sunol and Zia showed that subdiffusion, the category of anomalous diffusion where $\alpha < 1$, might be demonstrated within artificial cytoplasm by the use of more than one polymer length of PEG [1]. In their simulation, Sunol and Zia used extremely high concentrations of PEG at 20%, 30%, and 40% volume fractions. These concentrations are interesting in the context of

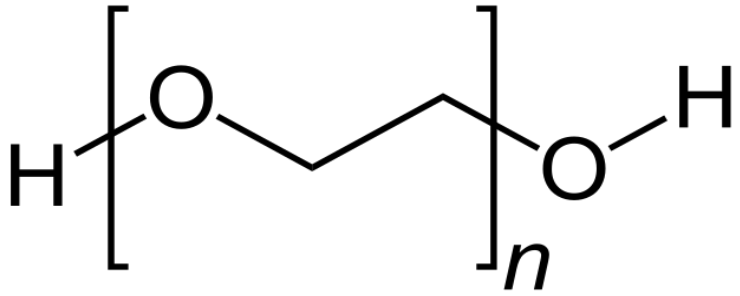

Figure 1: Polyethylene glycol (PEG) is an organic polymer of varying chain lengths and offers the potential for replicating biological cytoplasm's crowdedness in artificial environments.

Smolarsky's work given that the maximum water solubility for PEG is 50 mg/mL [11], which corresponds to a volume fraction of 2% within Smolarsky's aqueous solution. Consequently, the highest experimentally achievable volume fraction for PEG above 200 in length is only 10% of the lowest theoretical volume fraction studied.

3.1.2 Drift-Reducing Chambers

In order to better understand the mixing that occurs within the cytoplasm we are interested in the study of small-scale motion, including passive particle diffusion and active particle motion. Consequently, ensemble drift, referring to the collective slow movement towards something, is a considerable source of error. At such small scales, the separation of ensemble drift from particle diffusion or active motion can be difficult.

With the use of Janus particles in the fabrication of artificial cytoplasm, their chemical reaction creates a drift. The decomposition reaction of hydrogen peroxide, as seen in Eq. 1, produces water and oxygen. Given a high enough concentration of Janus particles, the volume of oxygen produced makes likely the creation of oxygen bubbles [5]. These bubbles create a rapid expansion in the medium, particularly when they move and merge, which introduces a large sample drift and consequent source of error.

In order to rectify this experimental challenge, Palacci designed a gel microsystem that allowed for the constant renewal of hydrogen peroxide fuel and the simultaneous removal of oxygen by diffusion through an agarose hydrogel [2]. Palacci's microfluidic device, Fig. 2, sandwiches the agarose gel between plexiglass, ensuring a proper seal of the system. Particles are introduced into central chambers in the gel prior to the sealing and a syringe pump is used to introduce hydrogen peroxide into the system.

Palacci's choice to use agarose hydrogel is particularly encouraging due to its unique, well-studied

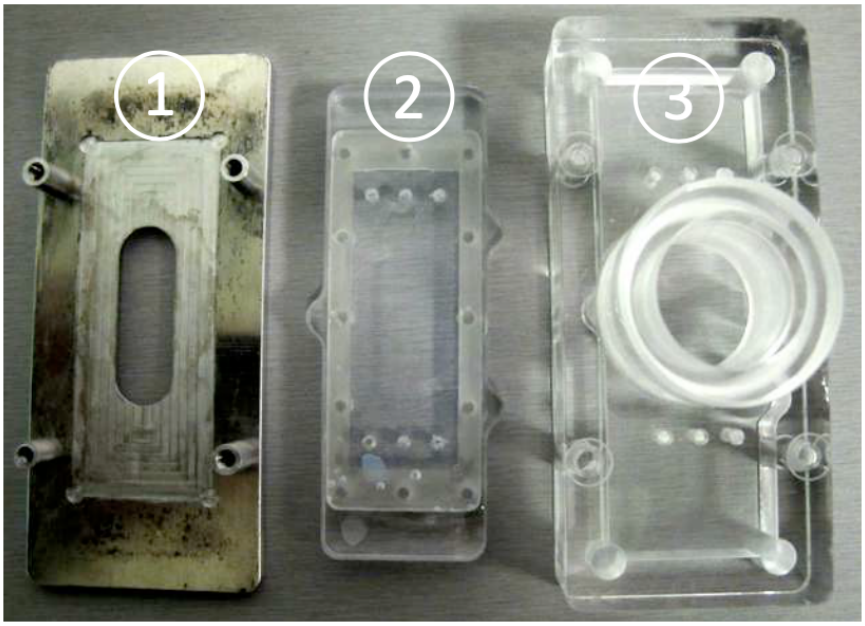

Figure 2: Photograph of the microfluidic device developed by Palacci et al. (2010) [2]. (1) is the metal framework, (2) is the plexiglass manifold that supports the agarose gel, and (3) is the plexiglass cover of the system which ensures proper sealing. Reprinted from [2].

structure. Often used in biology and chemistry to separate particles through gel electrophoresis, agarose hydrogel pores are large enough to enable the free diffusion of small molecules such as molecular oxygen, hydrogen peroxide, and water through the gel, yet small enough to contain the tracer and Janus particles within the gel.

Using his microfluidic device, Palacci demonstrated Brownian motion of particles within the agarose gel well. This signals that the device provided an environment free of convection from both internal and external causes. Despite this and the assurance of stable chemical conditions needed for the study of active colloids, Palacci's proposed device is difficult to replicate.

In his recent work, Smolarsky made initial strides toward the creation of a drift-reducing chamber that is easier to reproduce than Palacci's [10]. An agarose hydrogel, containing a central well, was sandwiched between a glass microscope slide and a perfusion chamber (Electron Microscopy Sciences) to seal the system from the exterior environment in an easier, and thus repeatable, fashion than Palacci. Commonly used in cellular biology, perfusion chambers are press-to-seal covers that form a water-tight seal when pressed to coverslips or microscope slides – similar to rubber gaskets. They have dual access ports that are designed for the quick addition or removal of reagents, Fig 3. Using this construction, Smolarsky identified the gel well boundary and took an initial measurement of the appropriate gel agarose height for seal formation. Despite

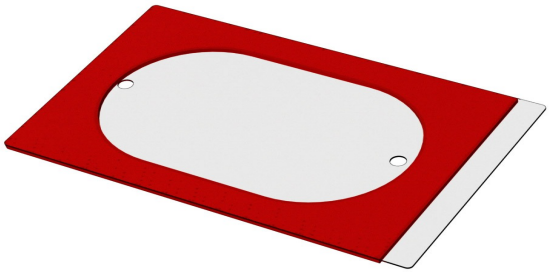

Figure 3: Image of a reusable CoverWell™ perfusion chamber made of medical grade silicone bonded to clear, UV-transparent plastic. Reprinted from [12]

the promising observed containment of particles within the agarose well, during the chamber assembly, there was air sealed within the space above the well interior due to a dimple in the agarose hydrogel, Fig. 4.

While the air pocket issue might be resolved by introducing more water into the system, which would theoretically push the water to diffuse through the hydrogel by the creation of an osmotic pressure gradient [2], this is not a given. The sole presence of an air pocket isn't itself problematic, but its potential to introduce evaporation into the system, which may create drift and thus impact particle stagnancy, is particularly concerning.

3.2 Goals

The overarching goal of this research is to further the existing study of passive diffusion and fueled particle motion in order to construct an artificial cytoplasm that mimics the functions and structures of a living biological cell. This exploration promotes a deeper understanding of biological processes and ultimately has extensive applications in a variety of fields.

More explicitly, this work will focus first on continuing the drift-reduction chamber construction started by Smolarsky. Given the potential for drift caused by the preexisting air pocket, the initial goal is to reconfigure the chamber to eliminate its presence. This process involves adjusting the agarose gel and sample preparation and construction to avoid entrapping air within the chamber.

Once the system is rid of trapped air, it must be demonstrated that it can be used to study particle

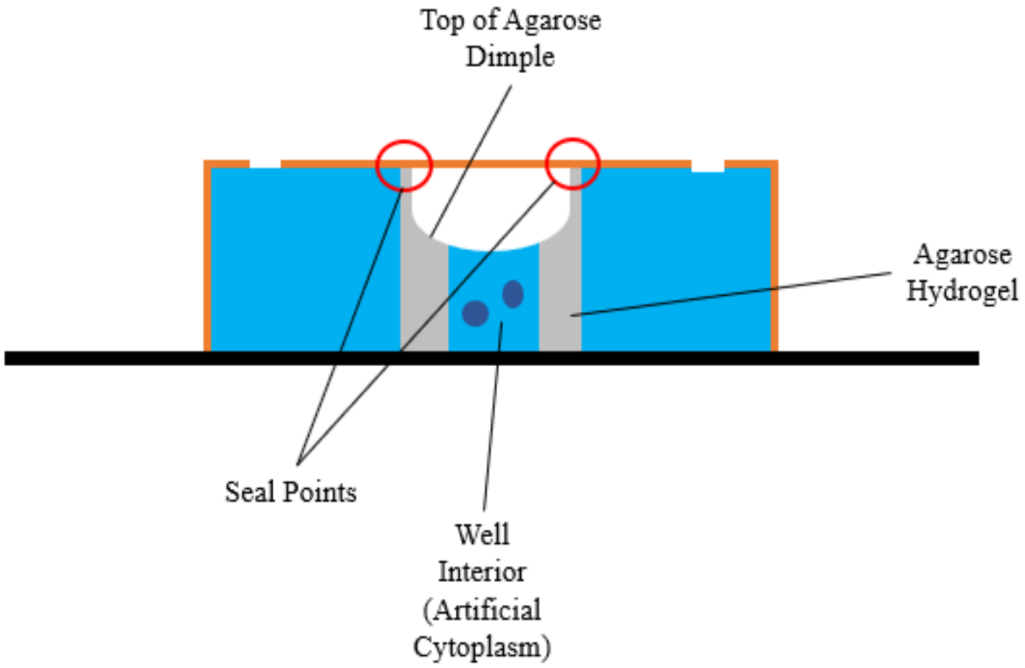

Figure 4: Side view of the contact seal created by Smolarsky with 2.05 mm tall agarose hydrogel. The agarose dimple shown was filled with air rather than sample solution contents when sealed. Reprinted from [10].

diffusion and active particle motion. In order to show this, the goal is to document tracer particle stagnancy within the agarose gel well. In his microfluidic device, Palacci was able to characterize the dynamics of individual swimmers and show that they maintained a persistent random walk, or Brownian motion [2]. The identification of Brownian motion suggests the sample is as stagnant as possible with minimum drift.

Alongside stagnancy, to be useful when studying Janus particles, the drift-reducing chamber must be shown to allow for the continual replenishing of fuel, H_2O_2, enabling a more convenient data-taking process that is not limited by the exhaustion time of the fuel. This ability will be studied by flowing fluorescently dyed water into the chamber.

These individual steps will help determine the feasibility of a perfusion-chamber-based drift-reduction chamber that may be used to more accurately study the diffusion of tracer particles and movement of fueled particles, ultimately furthering the study of artificial cytoplasm and promoting the understanding of biological cell environments.

In addition to the assessment of this drift-reduction chamber, this research will focus on polyethylene glycol as an artificial replication of a biological cell's crowdedness. While Smolarsky's findings did not demonstrate PEG's ability to replicate anomalous diffusion, Sunol and Zia's recent paper theoretically shows the potential of combining different polymer chain lengths. This work will follow their simulation, as is experimentally possible, to try to achieve anomalous diffusion, thus demonstrating PEG's ability to accurately replicate the crowdedness of biological cytoplasm.

Incorrect citation ~Viva

4 Theory

The theory of diffusion underlies the analytical work of observing and quantifying particle motion conducted in an artificial cytoplasm. On a large-scale, diffusion describes the tendency for particles to spread from areas of high concentration to areas of low concentration [13]. Individual particle movement, however, may also be described as diffusing.

4.1 Deriving Mean Squared Displacement: The Einstein Relation

One of the simplest meaningful statistical properties related to the study of particle dynamics is the mean squared displacement [6]. To derive this value, we begin by imagining a region where particle concentration, n, increases uniformly in one direction. The flux, $\vec{J}$, of particles across a surface in such a region may be described by Fick's second law [13]

$$J_x = -D\frac{dn}{dx} \tag{2}$$

where t is the time, the constant of proportionality D is the diffusion coefficient, and x is a coordinate. Published in his 1905 paper [14], Einstein found the solution to the above partial differential equation to be

$$n(x,t) = \frac{N}{\sqrt{4\pi Dt}} e^{-\frac{x^2}{4Dt}} \tag{3}$$

where N describes the number of particles diffusing in the medium. Einstein's solution mirrors the form of a general Gaussian curve function $f(u)$

$$f(u) = Ce^{-\frac{u^2}{2\sigma^2}} \tag{4}$$

where C is a constant, u is a variable input, and most importantly σ^2 is the variance of the function. Drawing comparison between Eq. 3 and Eq. 4

$$2\sigma^2 = 4Dt \tag{5}$$

$$\sigma_x^2 = 2Dt \tag{6}$$

determines the variance of Einstein's solution with respect to displacement, Eq. 6. The physical interpretation of this variance is the simplest meaningful statistical property related to particle motion: mean squared displacement (MSD). More directly, this variance represents the square of the average displacement that a particle has traversed from its starting point in one dimension. The resulting Einstein relation for MSD in one dimension is [14]

$$\langle x^2 \rangle = \sigma^2 = 2Dt \tag{7}$$

The additive nature of MSD allows for the easy computation of values in two and three dimensions. In two dimensions, say x and y, the MSD are $\langle x^2 \rangle = \langle y^2 \rangle = 2Dt$. The overall MSD for two-dimensional movement is therefore

$$\langle x^2 \rangle + \langle y^2 \rangle = 2(2Dt) = 4Dt \tag{8}$$

and for three-dimensional movement in the x, y, and z directions [Smolarsky]

$$\langle r^2 \rangle = \langle x^2 \rangle + \langle y^2 \rangle + \langle z^2 \rangle = 3(2Dt) = 6Dt \tag{9}$$

To make matters slightly more complicated, MSD must be specified as either relating to an individual particle, iMSD, or the ensemble of particles, eMSD. While iMSD allows for the very specific characterization of a single particle's motion, eMSD provides greater insight into the behavior of a collective group of particles and cytoplasm as a whole system. In this study, eMSD is used to characterize particle movement in artificial cytoplasm.

4.2 Diffusion Coefficient: The Stokes-Einstein Relation

The MSD equation leaves just one variable to be unpacked, the diffusion coefficient D, which is determined with the Stokes-Einstein relation. This relation begins with Fick's first law

$$J_x = -D\frac{\partial n}{\partial x} \tag{10}$$

which describes the flux of particles in one dimension across the surface of the previously proposed region, and Stokes' Law

$$F = 6\pi a\eta v \tag{11}$$

which describes the drag force exerted on spherical objects of small Reynolds numbers in viscous fluids. Einstein built upon Fick's first law using Stokes' Law to derive the following relation for the diffusion coefficient D [14]

$$D = \frac{RT}{6\pi N_A a\eta} \tag{12}$$

Understandably named the Stokes-Einstein relation [15], Eq. 12 defines R as the gas constant, T as temperature, N_A as the well-known Avogadro's number, α as the radius of the particles, and η as the medium's

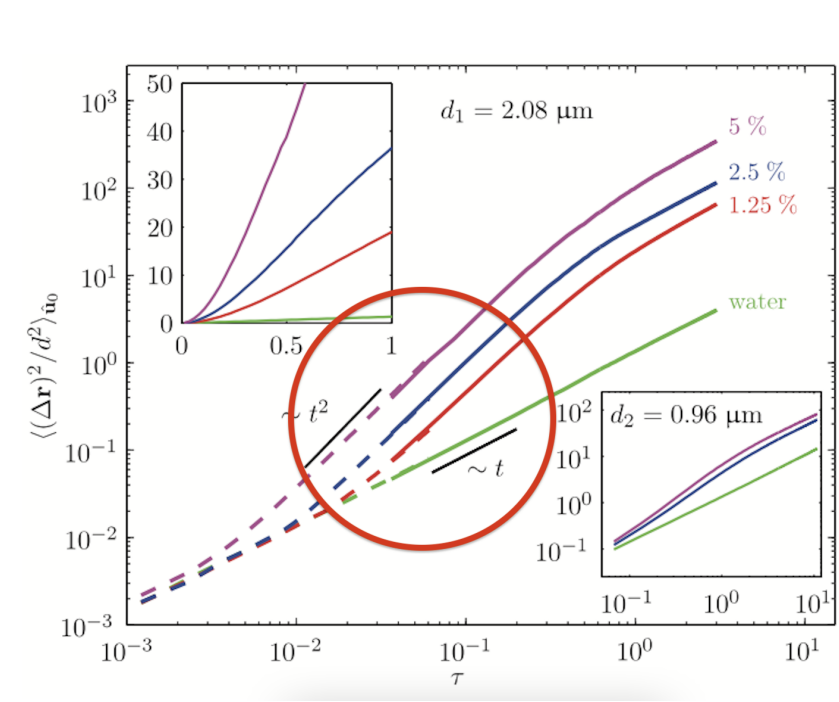

Figure 5: Log-log plot of Zheng et al.'s experimentally determined two-dimensional MSD values for Janus particles in water and various concentrations of H_2O_2 over a scaled time $\tau = D_r t$. Reprinted from [16].

viscosity.

Under the assumption of constant temperature and uniform particle radius, the Stokes-Einstein relation demonstrates that the medium's viscosity is the sole influence of a particle's diffusion coefficient and therefore said particle's MSD. More specifically, a larger diffusion coefficient correlates to enhanced diffusion, which may be expected in instances of fueled particle motion [5].

4.3 Anomalous Diffusion

A slight caveat to the above use of Fick's laws must be explored – they are designed for isotropic fluids in which properties are uniform throughout the medium [15]. As previously discussed, intracellular environments are complex, crowded mediums that therefore cannot be assumed to be isotropic.

A 2013 study by Zheng et al. (2013) [16] examined the motion of Janus particles in water and varying concentrations of H_2O_2. The MSD of Janus particles in these various mediums is shown in Fig. 5.

In such complex environments, a power law may be used to describe empirically useful data [15]. Such data includes values that fall within an easily observable time frame, as circled in Fig. 5. Using Eq. 8, the

corresponding power law is

$$\langle r^2 \rangle = 6Dt^{\alpha} \tag{13}$$

where α is the diffusive exponent. The diffusive exponent holds useful information about the type of diffusion observed. A value of $\alpha = 1$ corresponds to normal diffusion and results in the Stokes-Einstein relation, while a value of $\alpha \neq 1$ represents anomalous diffusion [15].

Anomalous diffusion, and the resulting deviation from the Stokes-Einstein equation, can be further characterized based on α value. Commonly encountered in constant velocity $x = vt$ scenarios, $\alpha = 2$ represents ballistic motion where $\langle r^2 \rangle \propto t^2$ [5]. Superdiffusion lies between normal diffusion and ballistic motion, where $1 < \alpha < 2$ [15]]. The final category of anomalous diffusion is subdiffusion which occurs when $\alpha < 1$ [15]. With the diffusive exponent, particle motion can be easily categorized and therefore better understood.

5 Methods

5.1 Agarose Gel Preparation

Gel preparation methods outlined by Palacci (2010) were followed to produce the agarose hydrogel cylinders used in the drift-reduction chamber [2]. A 4.5-5% agarose solution was created by combining 1.24 g of agarose hydrogel powder with 25 mL of RO water. This solution was vortexed for approximately 30 seconds until it appeared as a cloudy suspension. The solution was then transferred into a beaker and microwaved at 1.35 kW until boiling – approximately 30 seconds. After being stirred this process was repeated, being careful not to burn the solution, until the agarose was homogeneously dissolved in the RO water. The beaker was then covered with tinfoil to limit evaporation and settling during the next step.

The beaker was placed onto a hotplate with a magnetic stir bar (moving around 100-200 rpm) until the solution reached $80 - 90^{\circ}$ C. If a metal mold was used for the gel cylinders then it, too, was placed on the hot plate to avoid rapid cooling of the hydrogel in the next step. Once the solution reached the proper temperature it was poured into either an aluminum or Lexan mold with generally-cylindrical slots, the specifications of which will be discussed later on in section 6.1.2, directly after removing it from heat. The top of the mold was quickly scraped using a glass microscope slide to remove excess agarose and ensure a smooth flat surface. The agarose was then cooled to room temperature in the mold, allowing the hydrogel matrix to settle. The agarose hydrogels were then removed from the mold and stored in RO water while refrigerated at $2 - 8^{o}$C until ready for use.

Excess agarose may be reused by pouring it into a container and storing it without RO water at the same temperature to later be microwaved and heated according to the above procedure.

5.2 Observing and Quantifying Particle Movement

5.2.1 Bright-field and Fluorescence Microscopy

The observation and imaging of particles in this work was done using a Nikon Ti-E Inverted Microscope. Both bright-field and fluorescence microscopy were used to visualize small-scale objects. A quad filter was used during fluorescence microscopy to allow the observation of four different colors of fluorescent dye –

although red fluorescently dyed particles were primarily used. AVI videos were taken at 17.3 frames per second (fps) using a Thorlabs color camera.

While the two forms of microscopy used share many abilities, their technology and precision levels vary. Bright-field microscopy is the simplest technique using light microscopes, making it quite favorable. Visible light and magnifying lenses are used to view samples that appear as dark images on a bright background [17]. In this study, bright-field microscopy is primarily used to locate the boundaries of agarose hydrogel wells.

Fluorescence microscopy is a newer technique within light microscopy that allows for the targeted imaging of molecules that have been tagged with a fluorescent dye. This greater specification can occur because the unique quantum properties of the fluorescent particles cause them to be excited by a specific color light. This excitement results in the tagged particles giving off lower-energy light, with longer wavelengths [17]. It is this specific light wavelength, and thus color, that produces the magnified view seen by the viewer. Necessary to this project, fluorescence microscopy is used to locate and observe tracer particles and their movements. Unlike bright-field images that show particles as bright or dark, fluorescent images are simpler and our algorithm is able to identify the centroid of these very bright spots.

5.2.2 Video Analysis

In order to quantify the motion of particles in the artificial cytoplasm, we used a computer software program that could analyze recorded videos. The Python library TrackPy was used to study the motion of the fluorescently dyed tracer particles. This program works by locating the center of the particles and linking the coordinates of individual particles together into trajectories [18]. In addition to this, the overall ensemble drift of particles was calculated to separate the random movement, or Brownian motion, of particles from the collective motion of the system. The rotational and translational drift was modeled using a singular value decomposition (SVD) method and the resulting values were subtracted from the trajectories in order to obtain the drift-subtracted movement of the particles [5].

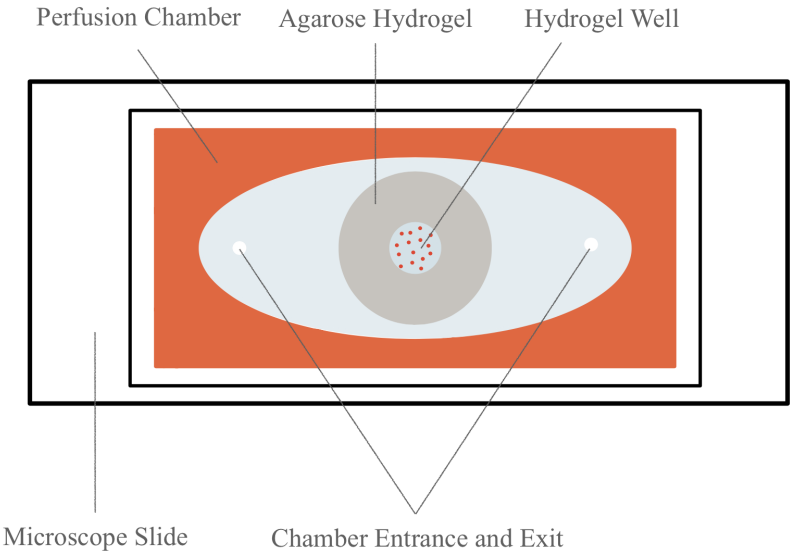

Figure 6: Top view of the generic drift-reducing chamber constructed throughout this project. *Not to scale

6 Drift-Reducing Chamber

The general components of the drift-reducing chamber remained the same from Smolarsky's work [10]: an agarose hydrogel cylinder, with a well in the center, was sandwiched between a microscope slide and a perfusion chamber. Pipetted into the well was 0.1 μL of fluorescently dyed sulfate latex tracer particles (Fluoromax, 1.1 μm diameter). The remainder of the drift-reducing chamber was filled with RO water to complete the device, Figs. 6 and 7. While these basic aspects were unchanged, many additional variables were tested to determine the most effective chamber construction, with the additional priority of eliminating the previously mentioned entrapped air bubble. These many components are outlined within this section.

6.1 Microfluidic Device Sealing

Leaks are a frequent, concerning problem in the realm of microfluidic devices. The smallest leak can prevent a device from functioning properly, and in certain instances cause concern for safety. Despite their prevalence, leaks are often difficult to pinpoint and even harder to fix. In order to create a chamber that is drift-reducing and can contain particles and the surrounding medium, it must be sealed properly and free from leakage.

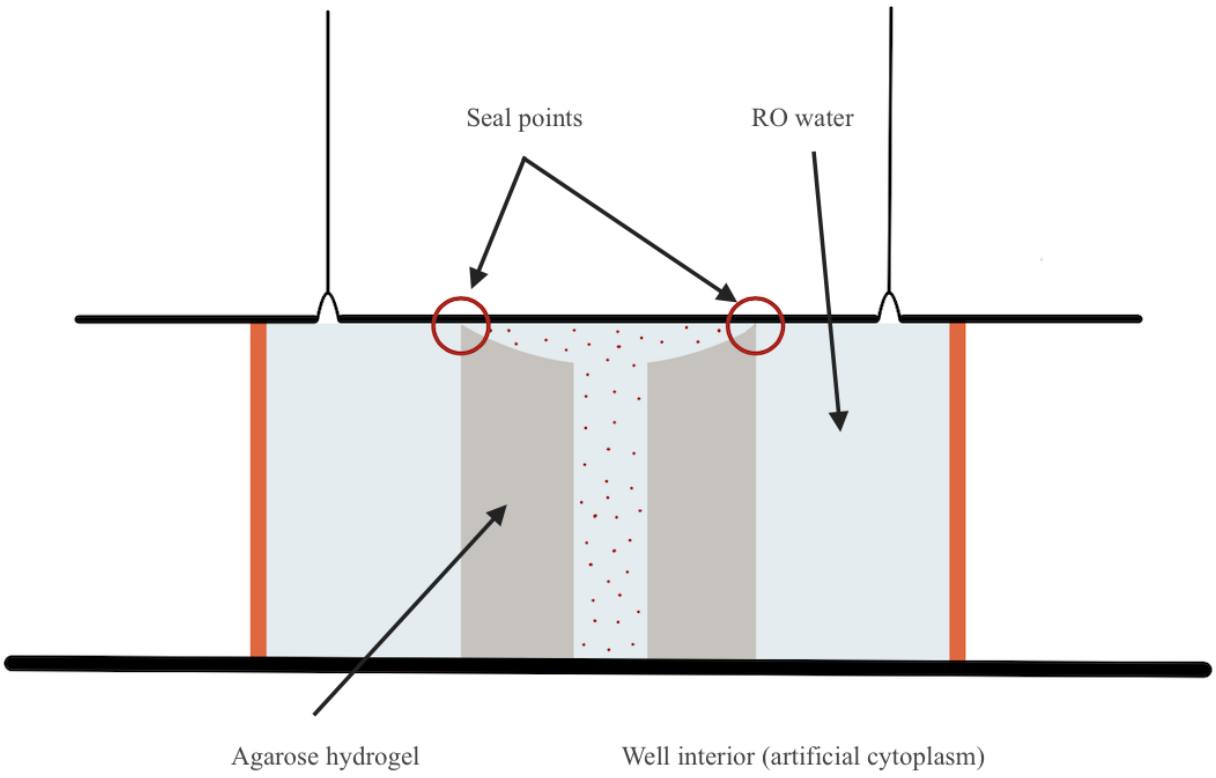

Figure 7: Cross section of the generic drift-reducing chamber constructed throughout this project. *Not to scale

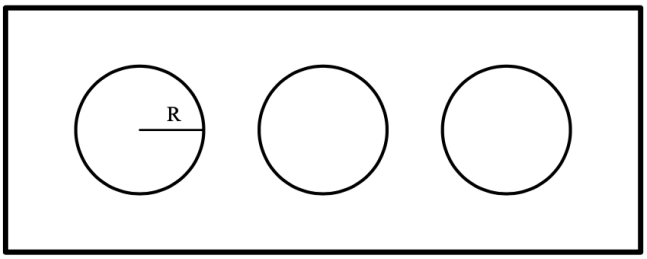

Figure 8: Top view of a theoretical agarose hydrogel mold. The radius, R, corresponds to the resulting hydrogel cylinder's radius.

6.1.1 The Issue of Hydrogel Swelling

With numerous applications to science, hydrogel's physical properties are well studied. In 2010, Roberts et al. published a comparative study of the viscoelastic mechanical behavior of agarose and PEG hydrogels in the context of cartilage tissue engineering [19]. Currently, Abigail Plummer et al. (2023) are studying the obstructed swelling and fracturing of hydrogels and their related agricultural function [20].

Despite the well-studied properties of hydrogels, during an initial attempt to construct a drift-reducing chamber without a dimple – using a freshly settled, flat-bottomed agarose gel cylinder – a major and unexpected problem was discovered. While it was known that agarose hydrogel absorbs water, its unexpectedly extensive expansion capabilities after settling caused it to swell above what was tolerated by the perfusion chamber seal. This swelling, more specifically referring to the volumetric-growth process that occurs when a porous material expands by spontaneous absorption of additional pore fluid [21], quickly created a large leak in the microfluidic device during the collection of data when the perfusion chamber gasket peeled off from the glass slide.

6.1.2 Characterizing Agarose Gel Swelling

In order to address this leak, the related swelling of agarose hydrogel needed to be characterized. Quantifying this characteristic involved measuring the height of an agarose hydrogel cylinder in RO water over a period of 24 hours. A flat-bottomed mold, Figs. 8 and 9, with depth d = 1.85 mm and radius R = 6.28 mm, was used to create an agarose cylinder according to the previously mentioned procedure.

Previous attempts to measure hydrogel height with a caliper depth rod proved difficult as the typical

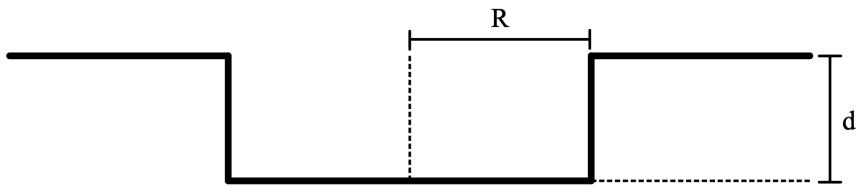

Figure 9: Cross-sectional view of a flat bottom agarose hydrogel mold. The radius, R, corresponds to the resulting hydrogel cylinder's radius, and depth, d, to its height.

Figure 10: Image of the developed measuring technique using calipers which allows for the measurement of soft agarose gel without distortion of the cylinder.

method of measurement placed too much pressure upon the hydrogel, causing it to crush under the weight of the caliper and produce an inaccurate measurement. Based on this experience, the measurement technique was adjusted and optimized according to Fig. 10. An initial measurement of the agarose gel height was taken directly after it was removed from the mold. The gel was then placed in a covered Petri dish with enough RO water to be submerged. In increments of 5 minutes, over a 60-minute period, the gel was momentarily removed from the Petri dish, measured, and replaced. Fig. 11 is a graphical representation of the agarose hydrogel height in mm over 60 minutes.

As seen in Fig. 11, the agarose gel undergoes most of its swelling within the first 10 minutes submerged in RO water, measuring 1.94 mm, 2.06 mm, and 2.14 mm at 0 min, 5 min, and 10 min respectively. After 10 minutes, the hydrogel reaches its maximum swollen height of around 2.14 mm $\pm$ 0.04 mm. Error in the height measurements is a result of the repeatability of measurements for the same hydrogel swelled cylinder.

This observation mirrors the results of Bertrand et al.'s 2016 study of the dynamics of swelling and drying in a spherical gel [21]. Their study's theoretical data is summarized in Fig. 12 and experimental data in Fig. 13. While the time duration before the plateau varies, the general behavior of the curve remains

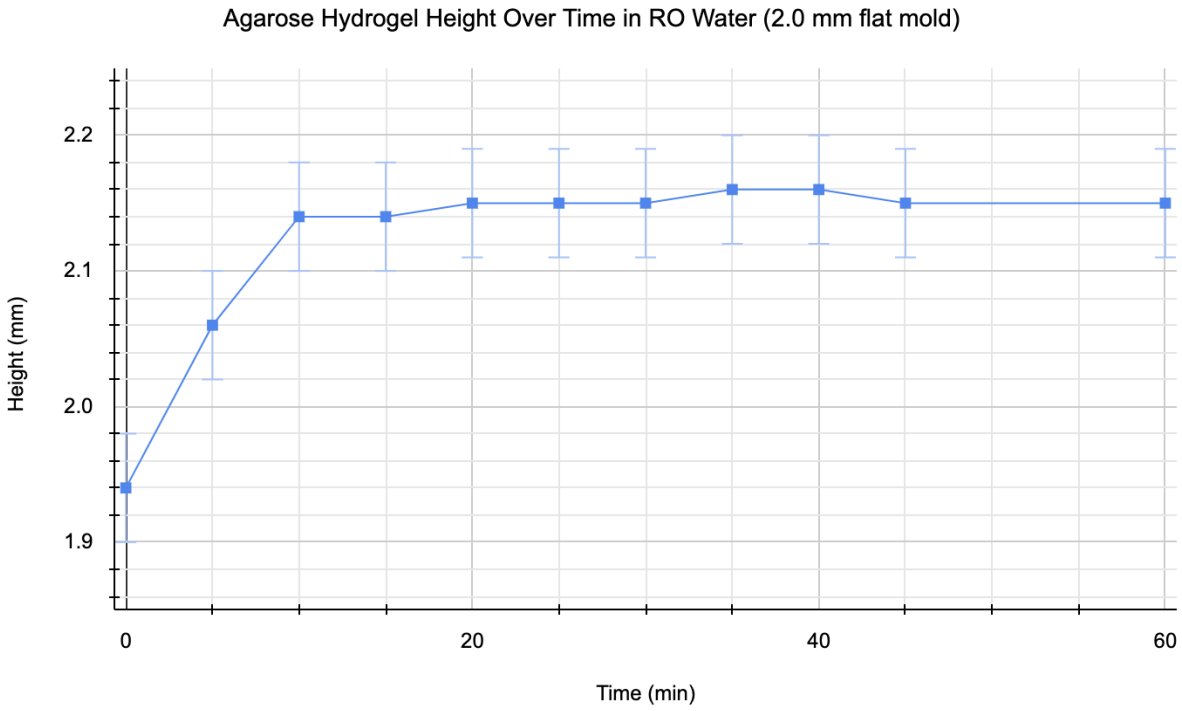

Figure 11: Experimentally determined values for an agarose hydrogel using a flat-bottomed mold with a depth of 2 mm. Measured heights are plotted against the time in which the agarose cylinder sat in RO water after being removed from its mold.

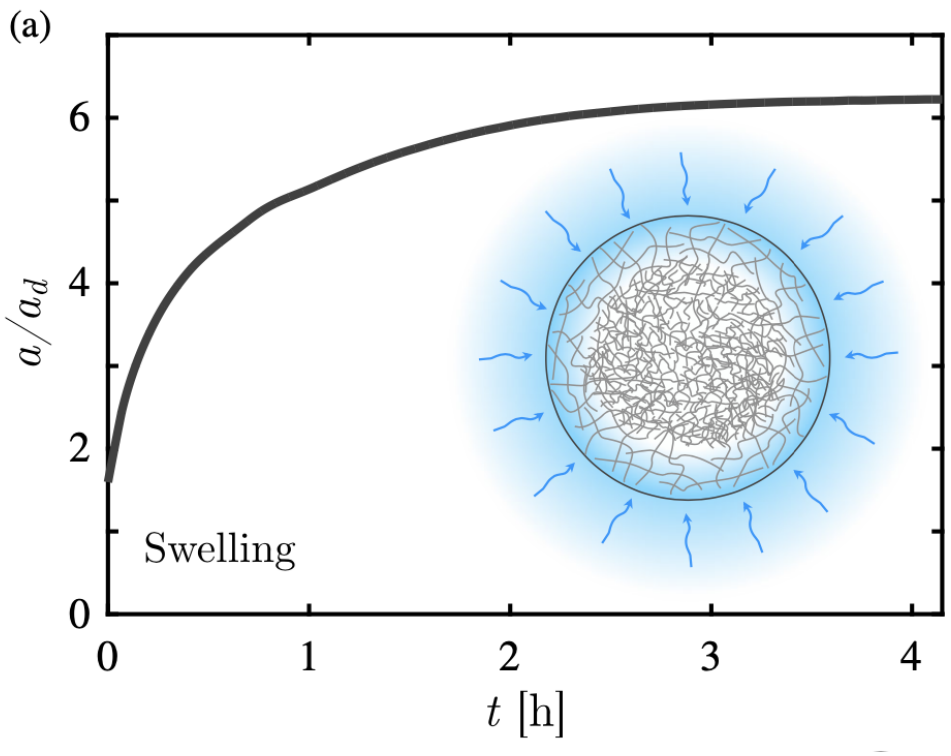

Figure 12: Illustrated representation of Bertrand et al.'s theoretically determined evolution of the mean radius of hydrogel beads with a dry radius $a_d = 0.76$ mm and a fully swollen radius of $6.4a_d$. Reprinted from [21].

similar. Given that swelling is dependent on object shape [21], it is likely that this time variation is a result of the difference between Bertrand et al.'s spherical gel and our cylindrical shape.

6.1.3 Resulting Agarose Gel Specifications

Storage:

In order to keep the experimental design as constant as possible during testing, the swelling test suggests that agarose hydrogels should be stored in RO water for at least 10 minutes prior to being used. This will allow for the gels to swell to their average maximum before they enter the chamber. While it is possible to allow this process to occur within the chamber, the contact between the microscope slide and the perfusion chamber top minimizes the hydrogel's exposure to water, slowing down the rate of swelling. Furthermore, it was observed that non-swollen fresh agarose may absorb the water from inside the well when allowed to swell within the chamber. This introduces problems as the center of the well dries up and the tracer particles become immobile.

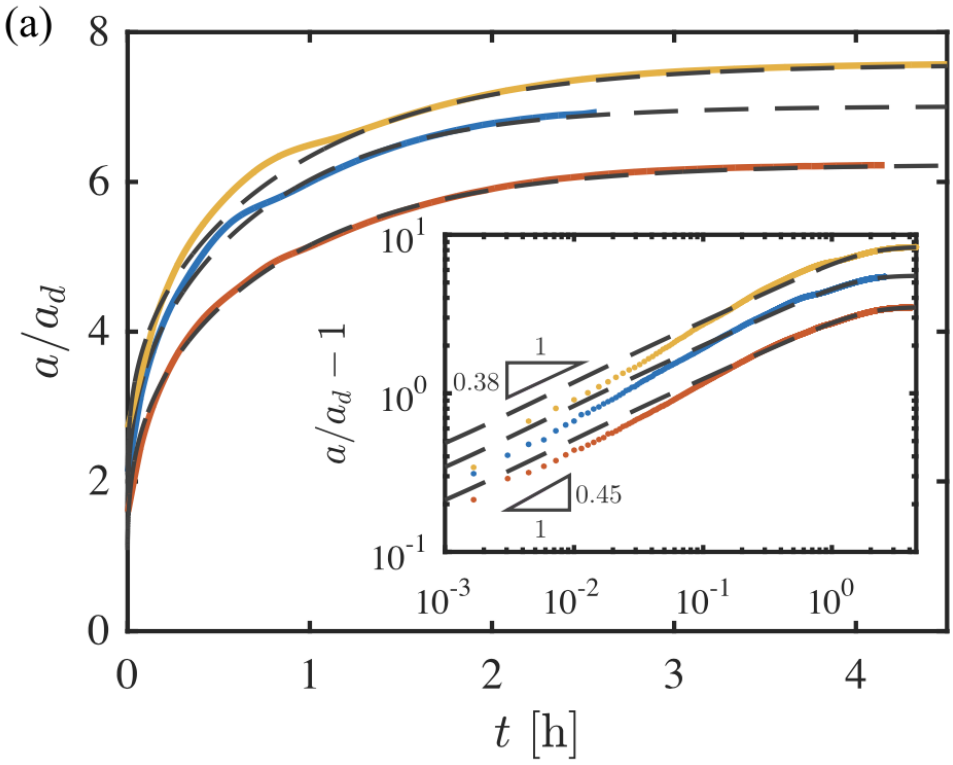

Figure 13: Graphical representation of Bertrand et al.'s experimentally determined time evolution of the radii of three hydrogel spheres after immersion in water. Experimental data are shown in colors with the predictions of the model depicted in dashed gray. Orange, blue, and yellow are all shifted vertically by 0, 0.5, and 1, respectively, for clarity. The same applies to their respective gray lines. The inset of the figure depicts $a/a_d - 1$ plotted against t on a logarithmic scale with each line scaled vertically by factors of 2/3, 1, and 3/2, respectively. Reprinted from [21].

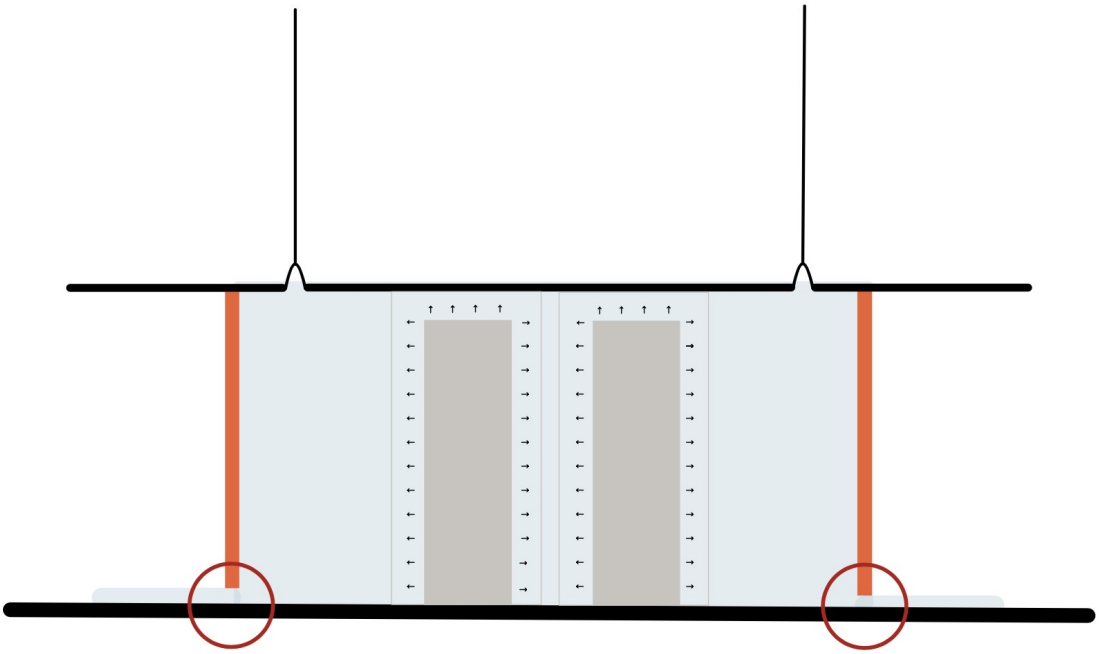

Figure 14: Representation of the theoretical mechanisms of flat-bottomed agarose swelling within a drift-reducing chamber. The swelling of the hydrogel places direct pressure on the perfusion chamber, causing it to unseal from the microscope as highlighted by the red circles. *Not to scale

Dimple Presence:

To get rid of the trapped air discussed in section 3.1.2, flat-bottomed molds were made to create agarose cylinders without dimpled ends. While these cylinders easily solved the problem of air entrapment, the fluctuating swelling of the agarose gels within the perfusion chambers was not tolerated by these samples. Figs. 14 and 15 demonstrate the theoretical "crunch zone" present in the dimpled agarose compared to the flat agarose – allowing for the small fluctuations in the volume of the dimpled agarose without the disruption of the gasket seal. Due to the ineffective gasket sealing that accompanied flat agarose, and this theoretical understanding of the dimple's crunch zone, it was determined that dimpled cylinders are preferable over flat ones. The resulting challenge became sealing the chamber without entrapping air while still using a dimpled hydrogel. The remedy to this complication will be explored below in section 6.2.

Height:

Within this study and Smolarsky's [10], discussed agarose hydrogel heights refer to a mold's label and intended depth. The actual depth of these molds varies slightly, although the order of their real depths

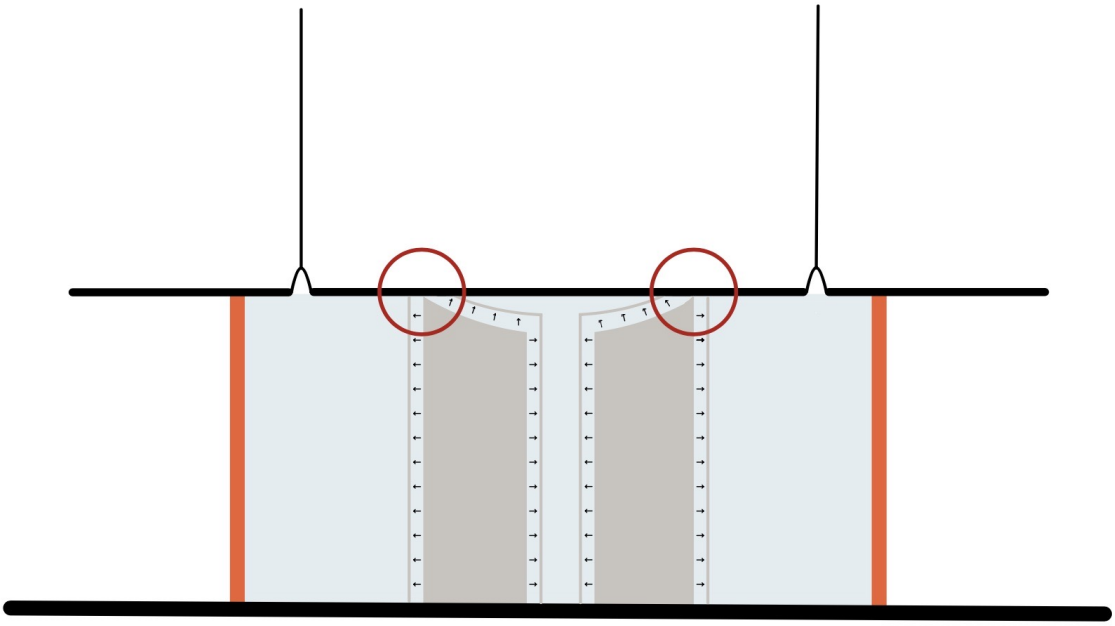

Figure 15: Representation of the theoretical mechanisms of a dimpled agarose hydrogel swelling within a drift-reducing chamber. Red circles enclose what may be understood as the "crunch zone" and allow for the fluctuation of agarose height caused by swelling. *Not to scale

matches the order of their intended depths. For ease and to match the language of Smolarsky's work, agarose hydrogel heights will be discussed with relation to their labeled height, however the following table outlines their realistic measurements.

Dimpled Agarose Mold: Actual Measurements		
Labeled/Intended Depth	**Edge Depth**	**Dimple Depth**
1.95	1.9	1.81
2.05	1.95	1.86
2.1	2.02	1.92

Table 1: Two depths are listed for each mold: the edge depth refers to the deepest point of the hydrogel mold along its perimeter while the dimple depth refers to the depth of the mold from the top of the dimple. Measurements were taken using a caliper depth rod.

Smolarsky concluded in his work that an agarose mold height of 2.05 mm was ideal given the equipment used in his study [10]. While the materials of this study remain the same, this gel height was tested again, now pre-swollen, to insure its correctness. An agarose gel height taller than 2.05 mm was also tested which was not previously done by Smolarsky.

As anticipated by the results of Smolarsky's data, the agarose gel height of 1.95 mm allowed for the perfusion chamber to seal against the microscope slide, but unfortunately was not tall enough to contain the tracer particles within the agarose well, Fig. 16a. Because agarose hydrogel floats in water, the stream of

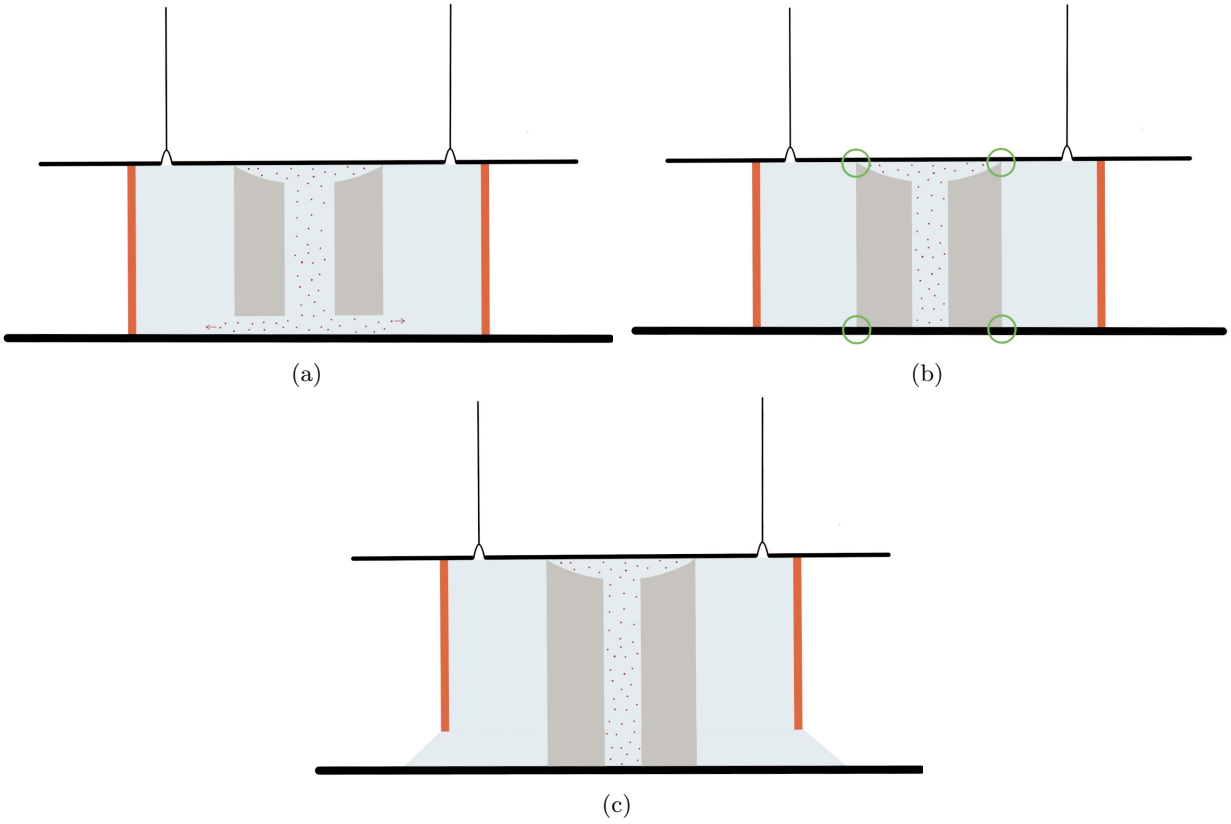

Figure 16: Illustrated representation of the results of varying agarose hydrogel heights. (a) depicts a drift-reducing chamber with an agarose hydrogel that is too short, 1.95 mm. The agarose floats within the chamber and allows particles to escape beneath it. (b) shows a properly fitted agarose hydrogel, 2.05 mm, with all four points of contact circled in green. (c) represents the instance in which the agarose hydrogel is too tall for the perfusion chamber, 2.1 mm. In this case, the hydrogel places pressure on the perfusion chamber top, causing the gasket to peel away from the microscope slide, allowing the contents to leak out.

tracer particles with the 1.95 mm can be seen escaping underneath the gel in Fig. 17a and was observed to be seeping outwards from the well. The 2.05 mm height, on the other hand, created a sealed environment and managed to contain the tracer particles within the agarose well, Fig. 16b. The containment of these particles is shown in Fig. 17b at a slightly higher height than the 1.95 mm cylinder. This is because the bottom-most layer of the 2.05 mm sample was only immobile particles that were trapped between the agarose and microscope slide when the device was sealed. This difference further highlights the 1.95 mm hydrogel's inability to create simultaneous contact with both the microscope slide and perfusion chamber.

To provide an upper limit on acceptable agarose hydrogel height, another chamber was constructed

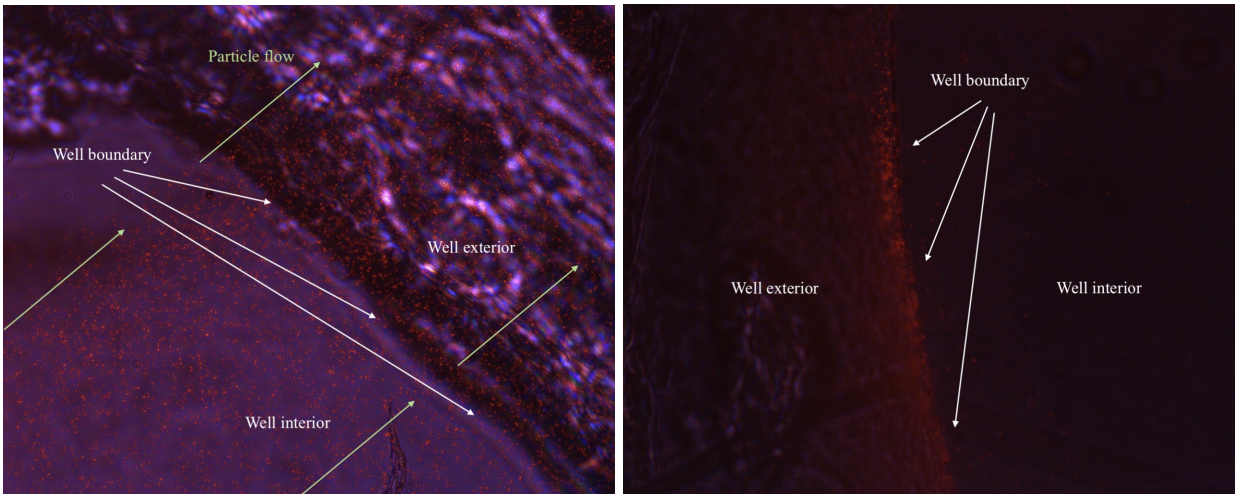

(a) 1.95 mm (b) 2.05 mm

Figure 17: Mixed bright-field and fluorescence microscope image of agarose hydrogel well boundaries using 10x magnification. The combination of both microscopy techniques allowed for the visualization of particles in context with the gel boundary and was possible in these images as the particles were not actively being recorded for analysis. Image (a) is that of a 1.95 mm agarose hydrogel. A stream of particles may be clearly identified here. Image (b) is of a 2.05 mm agarose hydrogel. A clear line of contained fluorescent tracer particles may be seen at the edge of the well.

using a cylinder of height 2.1 mm. While this height provided the same contact with the perfusion chamber as 2.05 mm, it was too tall to fit securely within the perfusion chamber. Consequently, the agarose lifted the sides of the perfusion chamber up from the microscope slide creating an unsealed and therefore unusable environment pictured theoretically in Fig. 16c and experimentally in Fig. 18.

6.2 Apparatus Construction

In addition to the hydrogel specifics previously mentioned, many other variables were tested throughout the construction of this drift-reducing chamber. These variables, their variations, and resulting conclusions are outlined in the table below.

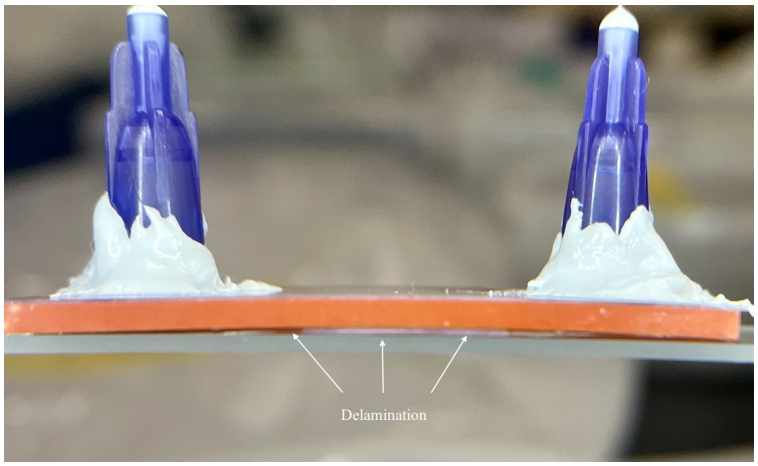

Figure 18: Photograph of the delamination between the microscope slide and the perfusion chamber gasket caused by the 2.1 mm agarose hydrogel cylinder height.

Tested Variables		
Variable Considered	**Tested Variations**	**Takeaways**
Flipped Construction	(1) Constructed with perfusion chamber on the bottom, filled with all components then sealed with microscope slide (2) Started with microscope slide and agarose, well filled with particles, then sealed with perfusion chamber and filled with RO water through inlet	Option (1) is favorable
Epoxy	(1) Devcon High Strength 5-minute Epoxy (2) PC-Products PC-11 Underwater 24 hr set Epoxy, two-part marine grade	Option (2) is preferred
Well Size	(1) Small hole of diameter 1.5 mm (2) Large hole of diameter 5.95 mm	Larger hole size (2) is best as it is easiest to pipette particles into
Tape	(1) Tape was placed on the short ends of the perfusion chamber (2) Tape was placed on all edges of the perfusion chamber (a) Regular household tape (b) Kapton film tape	The best combination was (2) and (b), yet no option fully sealed the chamber when pressure was applied

While the well size and use of tape may be easily interpreted, the flipped construction and epoxy are less straightforward. The testing of these more complex variables are further outlined below.

Flipped Construction

Following Smolarsky's procedure, initial drift-reducing chambers were constructed according to option (2). Despite the careful placement of the microscope slide to seal the device, an air bubble was still frequently trapped when using a dimpled cylinder. Flipping the device's construction order to option (1), which initially begun as an attempt to minimize construction time and reuse perfusion chambers with epoxied needle tips, proved to be a solution to the long standing air entrapment.

To achieve this building process a plastic stand was constructed to hold perfusion chambers with their needle tips pointing down. The subsequent construction steps are outlined in the graphics of Fig. 19.

Epoxy

During the manipulation of the perfusion chamber for flipped construction it was noted that the epoxy used by Smolarsky, Devcon high strength 5-minute epoxy, was quite brittle. Consequently, if the perfusion chamber was not handled delicately enough, or even slightly jostled during its filling, the needle tips would pop off of the chamber. Attempting to avoid this situation, it was found that 24-hour underwater epoxy, while it took longer to set, resulted in a more malleable hold.

6.3 Perfusion Chamber Limitations

Despite the promising gasket seal and containment of particles within the center well of the 2.05 mm hydrogel, major complications with the perfusion chamber were realized when fluorescent dye was flowed through the system.

In order to obtain reliable data for a fueled system without enclosed air, the syringe and tube used to introduce the dye must first be primed. The priming process, necessary in the construction of many micro and macro fluidic devices, involves applying pressure to the syringe plunger until the efflux of the fluorescent dye at the end of the tubing is visible. This process ensures the free flow of the solution once the pump is started and minimizes air introduced to the environment. Unfortunately, the presence of the needle tips on

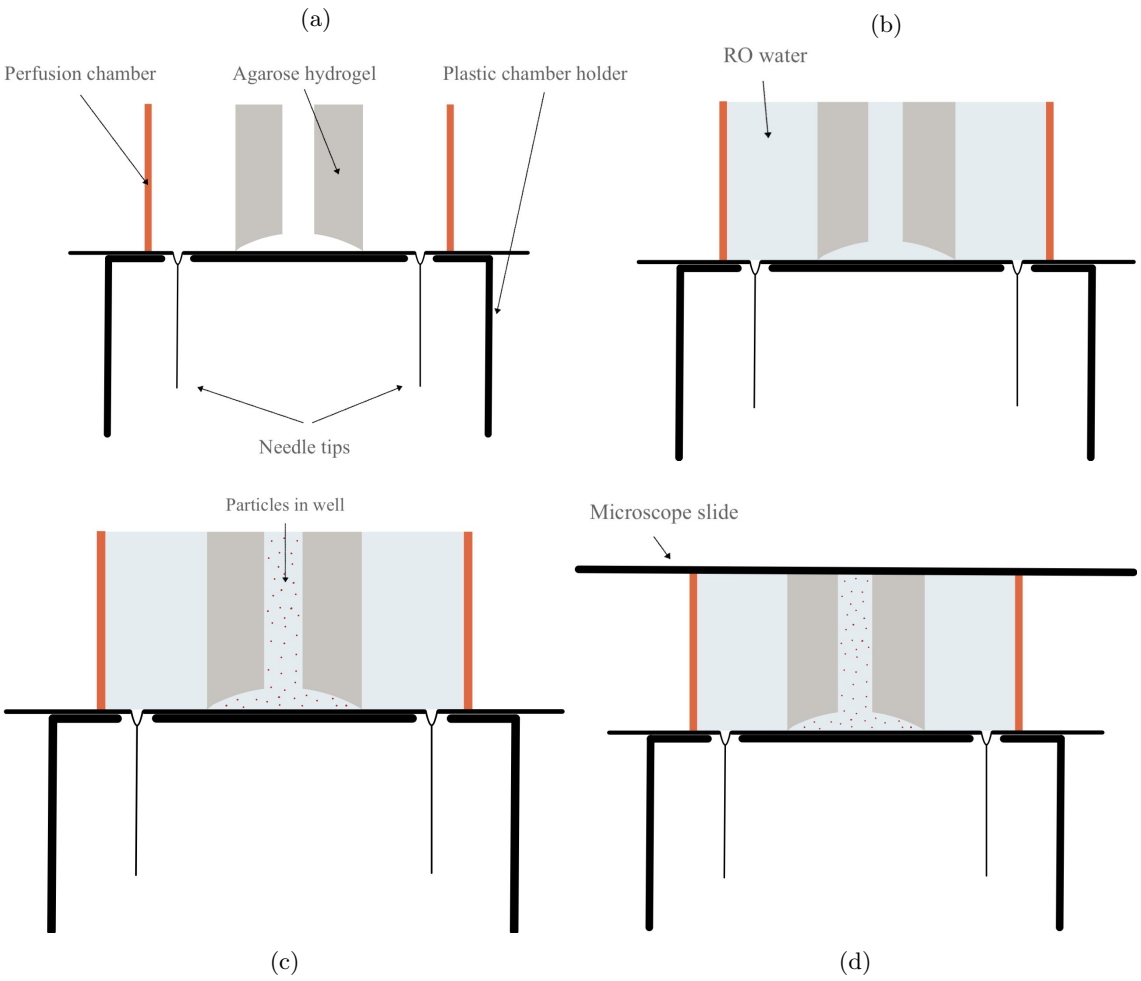

Figure 19: Cartoon representation of the flipped construction for the drift-reduction chamber. Step (a) requires the placement of a pre-set perfusion chamber and needles down on a plastic stand. The desired agarose hydrogel is then placed within the perfusion chamber. Next, (b) depicts the addition of RO water– this should completely fill the chamber. The introduction of the vortexed Fluoromax particles into the hydrogel well is shown in step (c). Finally, (d) illustrates the sealing of the device with a microscope slide.

the perfusion chamber introduce a challenge in that they cannot be primed before the device is fully built. As a result, all of the air from these needle tips must first be pushed through and out of the device before data may be collected.

After the tubing was primed it was gently attached to the needle tips on the perfusion chamber with careful attention to not disrupt the seal. Following this, an initial attempt to prime the needle tips was made by manually pressing the syringe forward. The pressure placed on the system by the quick addition of the dyed water proved to be too much for the fragile seal of the perfusion chamber, resulting in the immediate breakdown of the device. To combat the delamination of the device it was sealed with the different types of

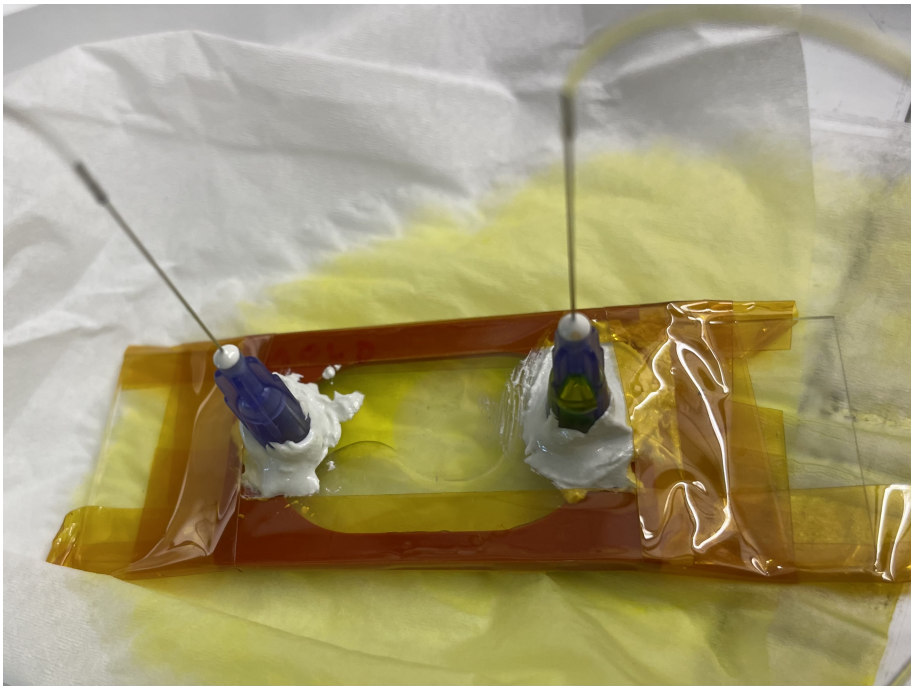

Figure 20: Image showing fluorescently dyed water, pumped using a Harvard PHD 2000 syringe pump at a speed of 30 μl/mn, leaking out of the separation formed between the perfusion chamber gasket and microscope slide.

tape mentioned in section 6.1. While the Kapton film tape was most effective in holding the system together, it was not strong enough to withstand the pressure from the manual priming.

A final effort was made to prime the microfluidic device and start a steady flow of fluorescently dyed water using the Harvard PHD 2000 syringe pump at a speed of 30 μl/mn. While this speed did not introduce nearly the same magnitude of pressure as the manual manipulation, it proved to still be too much for the gasket seal to handle and the perfusion chamber separated from the microscope slide as seen in Fig. 20 by the leakage of the dyed water.

Overall, despite the successful removal of trapped air from the agarose dimple, the inability to flow liquid through the drift-reducing chamber is a major setback. For the device to be useful in the study of the fueled motion of Janus particles and their effect on tracer particle motion, it is imperative that hydrogen peroxide fuel can be introduced to, and ideally flowed through, the sealed system.

7 Experimental Design: Tracer Diffusion and PEG

While the construction of an easily reproducible drift-reducing chamber that permits the study of Janus particles alongside tracer diffusion is still in the works, tracer particles themselves do not yield the same molecular oxygen byproduct and can therefore be studied in an enclosed space. A simple sealed slide that allows for the study of tracer particle motion within a variety of artificial environments and minimal drift is outlined below. As previously stated, Smolarsky was only able to identify basic diffusion of tracer particles, where $\alpha = 1$, with solutions using one polymer chain length of PEG [10], while the theoretical work of Sunol and Zia suggested anomalous diffusion to be possible using two different polymer chain lengths [1]. Sections 7, 8, and 9 explore the study of tracer particles in aqueous systems containing two separate polymer chain lengths of PEG in an attempt to experimentally create a more realistically crowded cytoplasm.

Incorrect citation. ~Viva

Given time constraints, polymer chain length combinations of this study were limited to 2000 and 8000 as well as 200 and 20000. While these combinations do not encompass all those possible, they are representative of both a drastic length difference and a small length difference between the two PEG lengths.

In addition to PEG length, the studied concentration in this work were carefully considered. Influenced by the high volume fractions of Sunol and Zia's study (20%, 30% and 40%) [1], this work focused only on the highest few possible concentrations of PEG. Both sets of polymer lengths were examined at 16.7 mg/mL, the highest concentration used by Smolarsky. They were also studied at a concentration of 25 mg/mL– the maximum possible concentration within the slide's aqueous solution given the previously discussed water solubility of PEG lengths above 200. Finally, PEG polymer length 200 is unique in that it comes in a liquid form which allows for its use at much higher concentrations. Consequently, the 200 and 20000 lengths could also be studied when holding 20000 at its highest concentration and introducing pure liquid 200 PEG to the solution.

7.1 Apparatus and Slide Construction

To create the sealed sample slides, a 9 mm diameter secure seal spacer (Electron Microscopy Sciences) is placed on a microscope side and 4 μL of mineral oil is pipetted into its center. Tracer particles are vortexed and 1 μL is added to an Eppendorf tube. Also added to the Eppendorf tube are 0.5 μL each of two PEG chain lengths (2000 and 8000, or 200 and 20000) at varying concentrations (both 50 mg/mL or 200 PEG

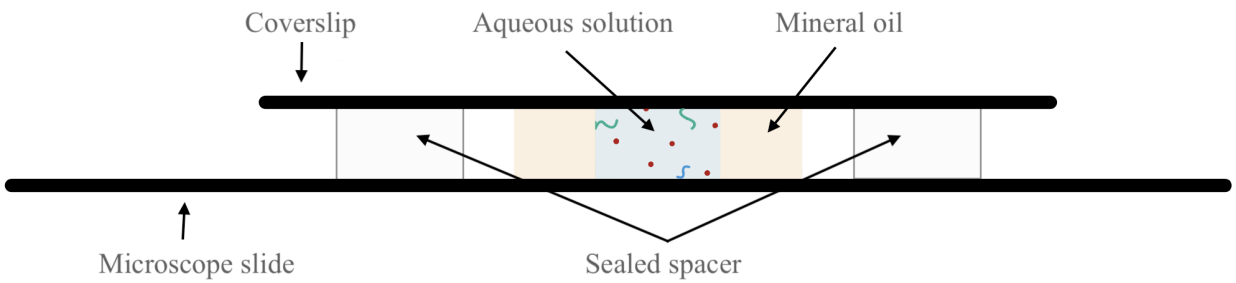

Figure 21: Cross-sectional view of a sealed sample slide. *Not to scale

at full concentration and 20000 at 50 mg/mL). The contents of the full aqueous solution bring the effective concentrations of PEG down by a factor of 2. To introduce another level of concentration, both sets of PEG lengths are also tested using 50 mg/mL concentration, but an additional 1 μL of RO water is added to the Eppendorf tube, reducing their effective concentration by a factor of 3 rather than 2.

The contents of the Eppendorf tube are vortexed for 30 seconds to ensure proper mixing and pipetted into the center of the mineral oil droplet that already exists on the microscope slide. Occasionally small bubbles are inadvertently introduced into the aqueous solution during the pipetting process. These bubbles can be easily popped using the tip of a needle. Lastly, a coverslip is carefully placed on top of the slide and solution to seal it off, Figs. 21 and 22.

7.2 Methods

Following the construction of a sealed sample slide, tracer particle motion was recorded at 17.3 fps and 40x magnification using fluorescence microscopy according to section 5.2.1. For each slide, three separate videos of approximately equal lengths were recorded at different locations within the aqueous solution to account for sample variations over time and space. The recorded videos were then analyzed with TrackPy software [18] as described in section 5.2.2.

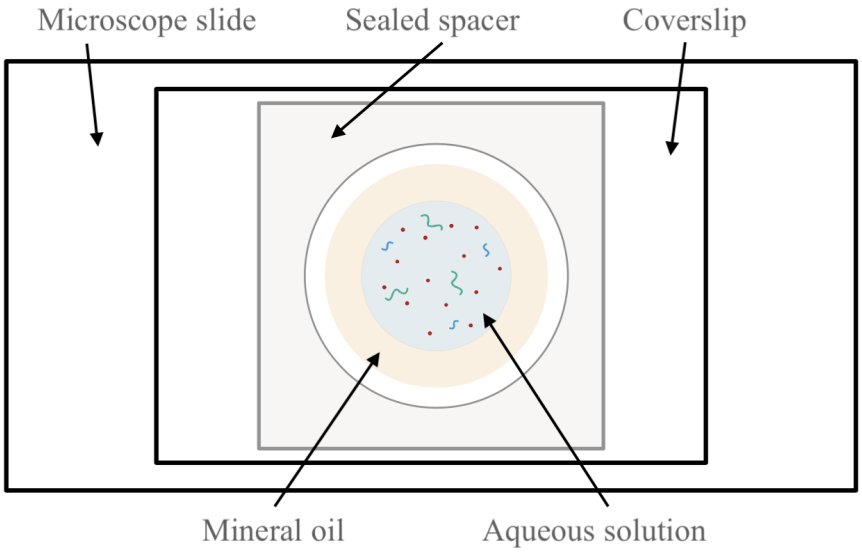

Figure 22: Top view of a sealed sample slide. *Not to scale

8 Results: Tracer Diffusion and PEG

To complete an analysis of particle diffusion, the TrackPy software locates the centroid of each individual fluorescent particle and maps its trajectory, as seen in Fig. 23. Measured particle trajectories are then modified by subtracting drift, a measurement for which is seen in Fig. 24. The resulting trajectories are used to calculate both iMSD and eMSD. The graph for iMSD, Fig. 25, while interesting, is less useful than the resulting eMSD graphs. As previously mentioned, eMSD provides greater insight into the cytoplasm as a whole system. Thus, eMSD, and related values, were the focus of studying tracer diffusion in this work.

A sealed sample slide was created for each possible combination of PEG concentrations and PEG polymer chain lengths. For PEG lengths of 200 and 20000 each at 25 mg/mL, two additional slides were made. This larger set of experimental data showed the findings explored in this section to be reproducible.

8.1 MSD and Log Plots

For each video recorded, TrackPy analyzed the motion of tracer particles and measured eMSD [μm^2] values over time [s]. Figs. 26a and 26b are eMSD graphs for both sets of PEG lengths at the lowest concentration studied, 16.7 mg/mL. eMSD graphs for the middle concentration of 25 mg/mL, based on the

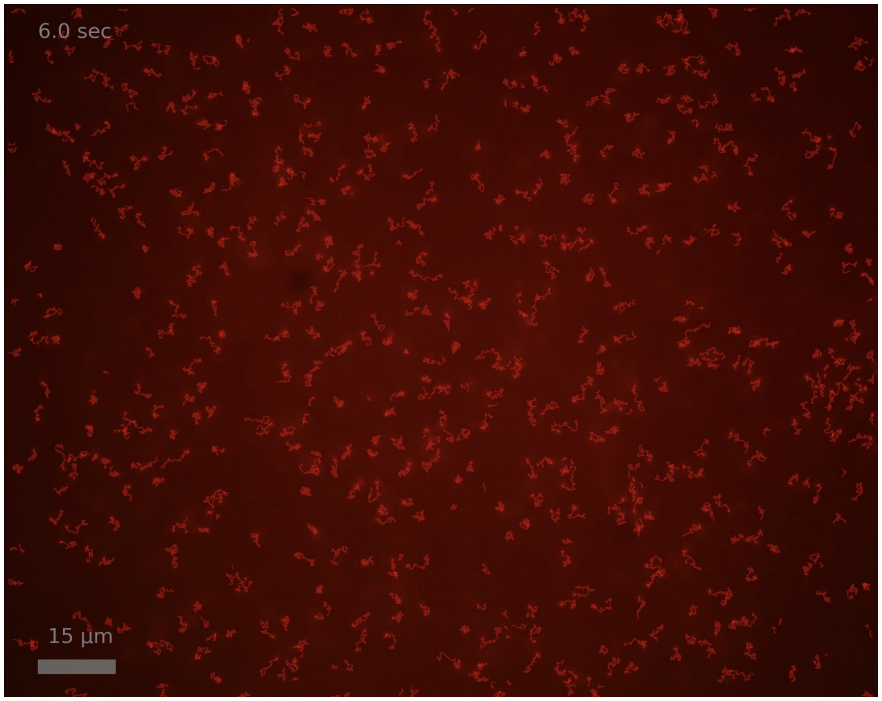

Figure 23: TrackPy [18] particle trajectory for an aqueous solution with PEG of lengths 200 & 20000 at 16.7 mg/mL concentration after 6.0 seconds.

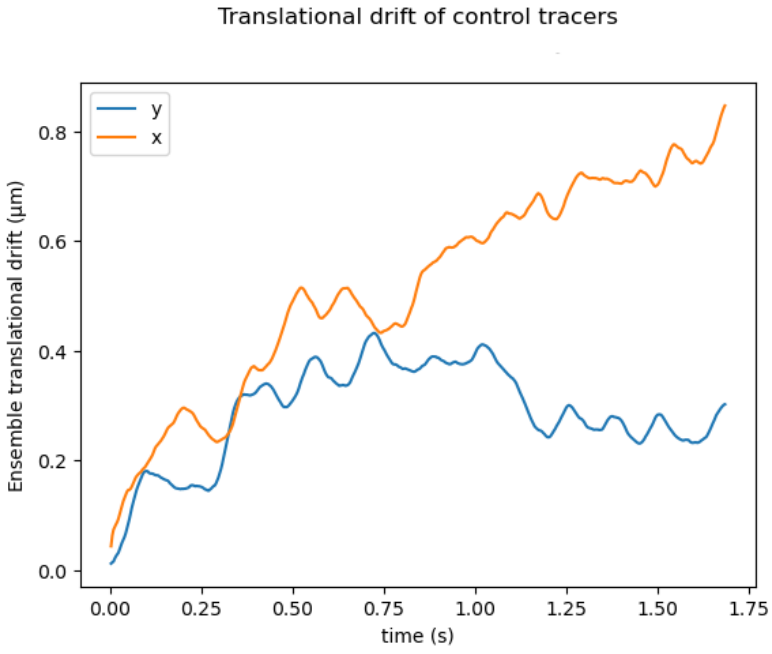

Figure 24: TrackPy [18] graph of ensemble translational drift of tracer particles over time for an aqueous solution with PEG of lengths 200 & 20000 at 16.7 mg/mL concentration.

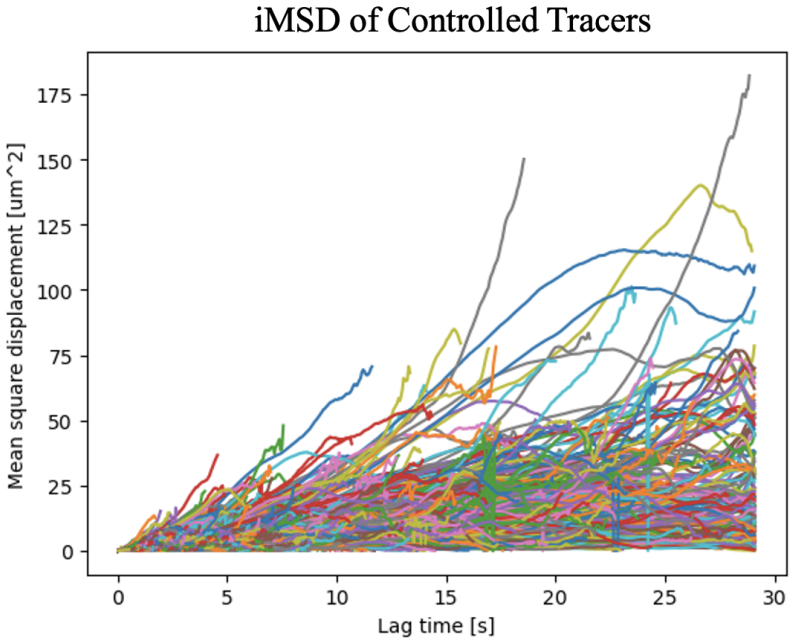

Figure 25: TrackPy [18] graph of iMSD for control tracer particles over time. Data was collected from an aqueous solution with PEG of lengths 200 & 20000 at 16.7 mg/mL concentration.

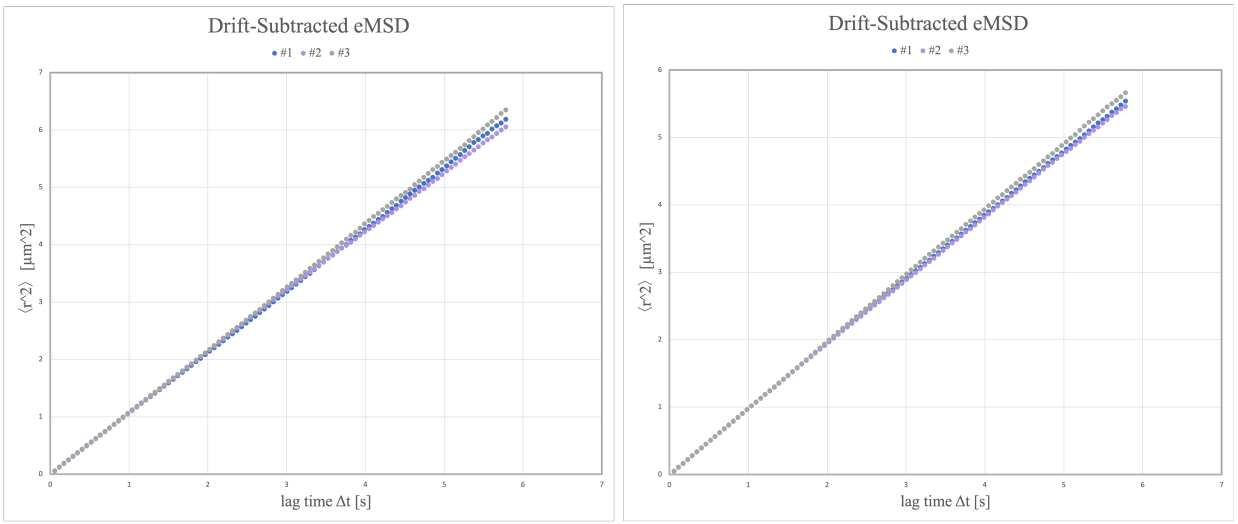

(a) (b)

Figure 26: Experimentally determined eMSD values over lag time for the recorded videos of sealed sample slides at concentration **16.7 mg/mL** concentration and PEG lengths (a) 2000 & 8000 and (b) 200 & 20000.

maximum solubility of PEG, are shown in Figs. 27a and 27b. The final eMSD plot over lag time at the highest studied concentration is Fig. 28. As mentioned prior, this high concentration is made possible by the liquid state of PEG polymer length 200.

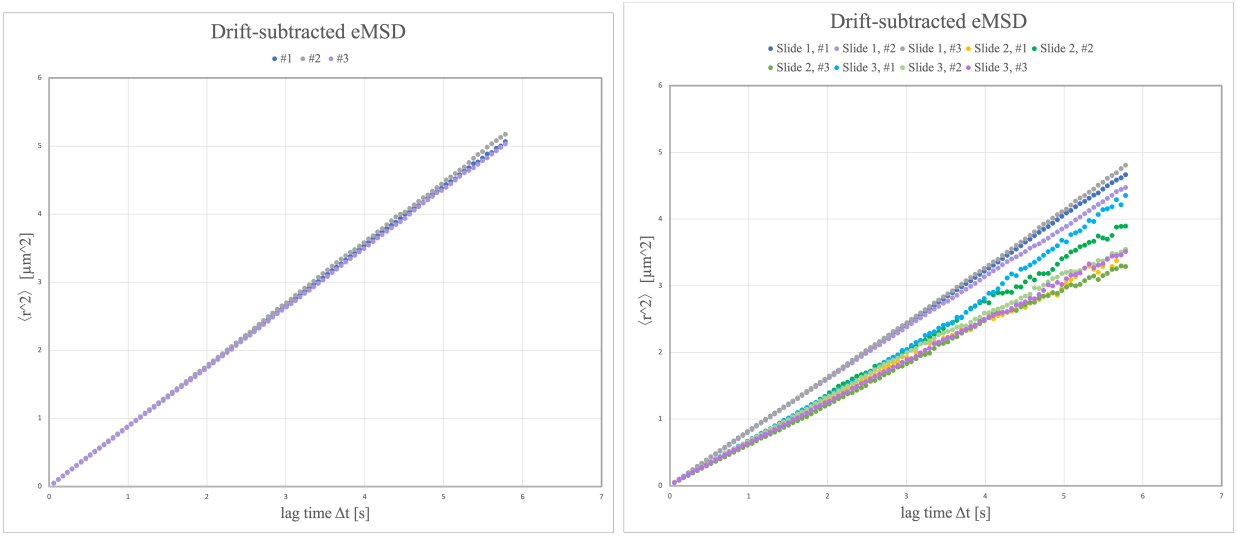

(a) (b)

Figure 27: Experimentally determined eMSD values over lag time for the recorded videos of sealed sample slides at concentration **25 mg/mL** concentration and PEG lengths (a) 2000 & 8000 and (b) 200 & 20000.

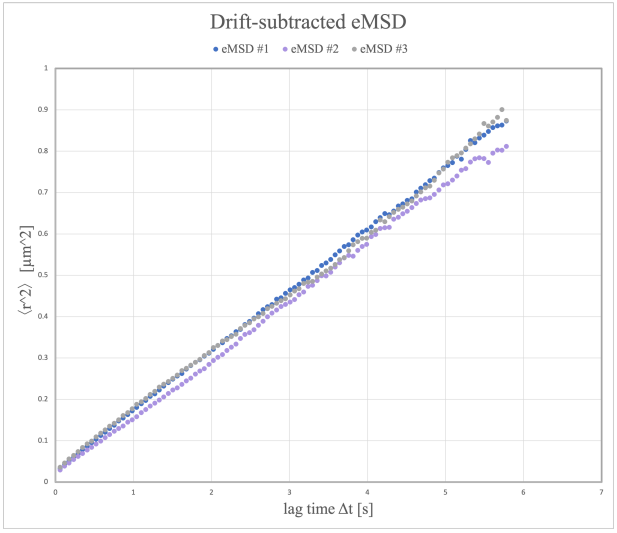

Figure 28: Plotted eMSD values over lag time for the recorded videos of the sealed sample slide with PEG length 200 at **40% volume** concentration and 20000 at **20 mg/mL** concentration.

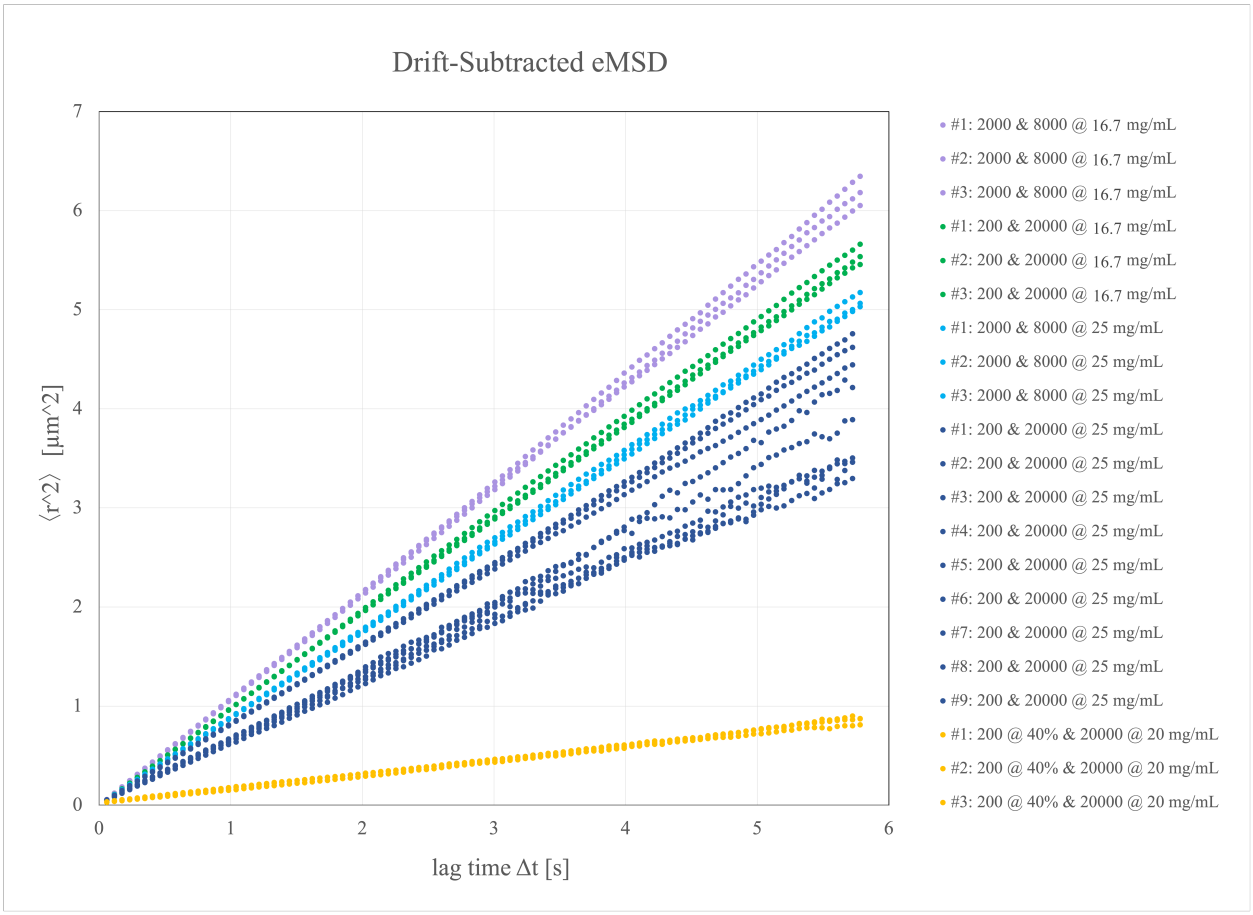

Figure 29: Experimentally determined eMSD values over lag time for all recorded videos. This graph encompasses the five concentration and PEG length combinations studied in this work: PEG 2000 & 8000 at 16.7 mg/mL, PEG 200 & 20000 at 16.7 mg/mL, PEG 2000 & 8000 at 25 mg/mL, PEG 200 & 20000 at 25 mg/mL, and PEG 200 at 40% volume concentration & PEG 20000 at 20 mg/mL.

In addition to the eMSD plots for each recorded video at a given concentration and PEG chain length combination, all of the eMSD data collected is collectively summarized into one graph, Fig. 29. Generally, as the PEG concentration increased, the slope of the eMSD plot decreased. Additionally, for each concentration, as the difference between the two included PEG polymer chain lengths increased, the slope of the eMSD plot decreased.

The eMSD plots in Figs. 26, 27, and 28 are somewhat linear. Consequently, TrackPy is designed to take advantage of this and create log-log plots of the logarithm of MSD versus the logarithm of time for the videos analyzed [10]. Fig. 30 is the $\log_{10}$-$\log_{10}$ plot for all measured eMSD. Taking the logarithm of both sides of Eqn. 9

$$log\langle r^2\rangle = log(6Dt^{\alpha}) \tag{14}$$

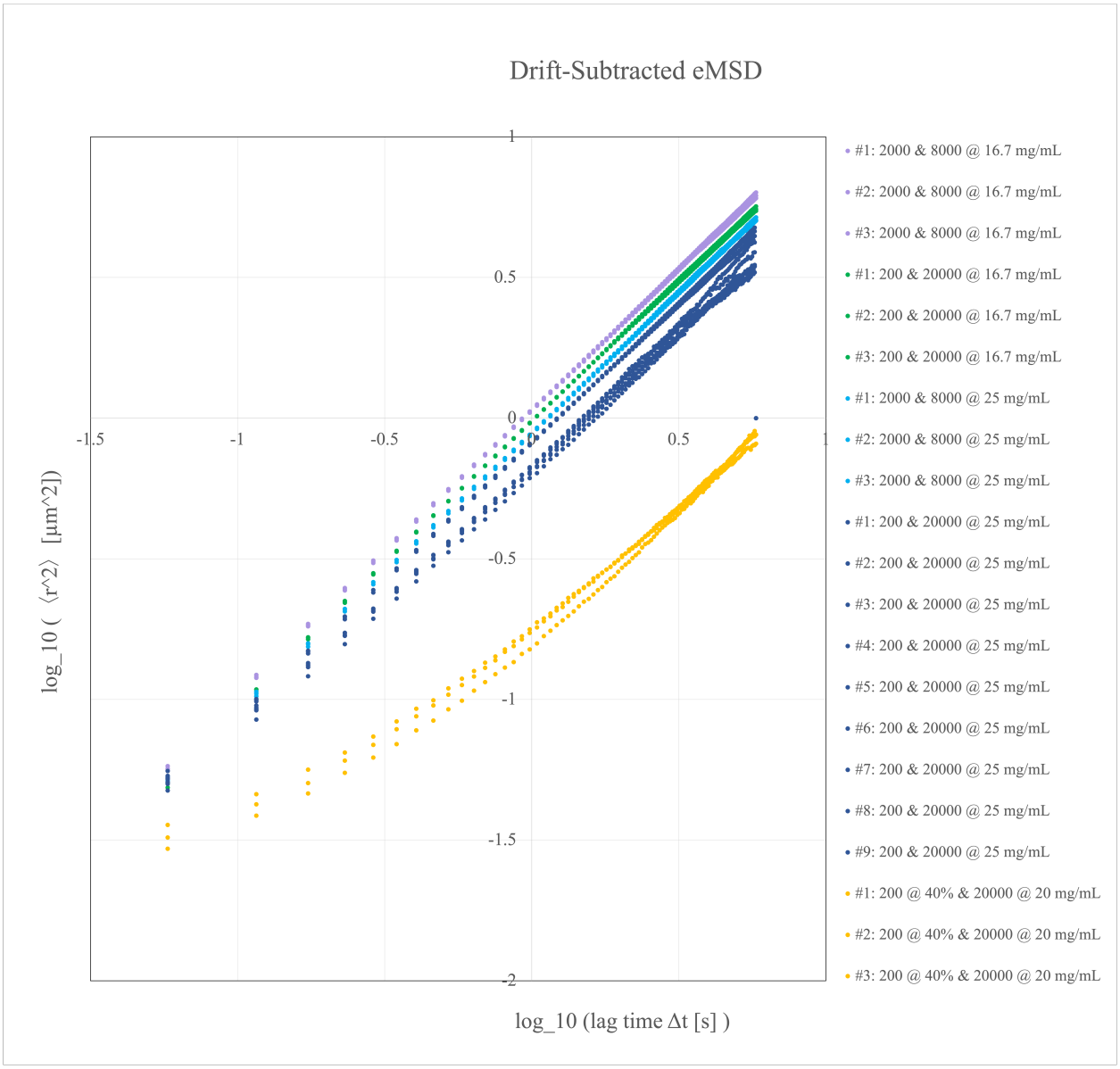

Figure 30: Log_{10}-$\log_{10}$ plot of the experimentally determined eMSD values over lag time for all recorded videos. This graph encompasses the five concentration and PEG length combinations studied in this work: PEG 2000 & 8000 at 16.7 mg/mL, PEG 200 & 20000 at 16.7 mg/mL, PEG 2000 & 8000 at 25 mg/mL, PEG 200 & 20000 at 25 mg/mL, and PEG 200 at 40% volume concentration & PEG 20000 at 20 mg/mL.

and recalling logarithm rules

$$log(MN) = log(M) + log(N) \tag{15}$$

$$log(M^k) = k\ log(M) \tag{16}$$

allows for the following reframing of Eqn. 9 in correspondence with the log-log plot:

$$log\langle r^2 \rangle = \alpha\ log(t) + log(6D) \tag{17}$$

where α, the diffusive exponent, is the slope of the log-log plot, and $log(6D)$ is the y-intercept. Using this manipulation, the software calculates a diffusion coefficient A and diffusive exponent α. It must be noted that the general diffusion coefficient produced by this software, A, does not consider the numerical factors that are used to determine the true diffusion coefficient, D, in the Einstein, Eq. 3, and Stokes-Einstein, Eq. 12, relations [10]. Given the two-dimensional nature of the video recordings, a more representative equation for the log-log plots given by this software's analysis is

$$log\langle r^2 \rangle = \alpha\ log(t) + log(A) \tag{18}$$

where $A = 4D$.

8.2 Diffusion Coefficients and Diffusive Exponents

Measurements of diffusion coefficient, A, and diffusive exponent, α, in aqueous solutions with various concentrations and polymer chain lengths of PEG are summarized in the tables below.

Sample Slide Coding System		
Sample Code	**Sample Description**	**Number of Contributing Slides**
1	PEG 200 & 20000 @ 16.7 mg/mL	1 slide (3 videos)
2	PEG 2000 & 8000 @ 16.7 mg/mL	1 slide (3 videos)
3	PEG 200 & 20000 @ 25 mg/mL	3 slides (9 videos)
4	PEG 2000 & 8000 @ 25 mg/mL	1 slide (3 videos)
5	PEG 200 @ 40% volume & 20000 @ 20 mg/mL	1 slide (3 videos)

Table 2: Table of the sample slide coding system used to organize the measured α and A values in Tables 3

and 4.

Diffusive Exponent, α		
Sample Code	**Average α**	**Uncertainty in α**
1	1.004	0.006
2	1.005	0.009
3	0.966	0.015
4	0.996	0.002
5	0.82	0.02

Table 3: Experimentally determined average diffusive exponents, α, for each of the five possible PEG concentration and polymer chain length combinations in the aqueous solution. Individual data points that make up the average can be found in **Appendix 2 - 6**.

In aqueous solutions with mixed PEG chain lengths, the measured diffusive exponent of tracer particles, α, notably decreased with increased PEG concentration. Furthermore, α similarly decreased with an increase in the difference between the included PEG polymer chain lengths– i.e. the more drastically different the PEG lengths are within an aqueous solution, the lower the diffusive exponent α.

Focusing more specifically on the measured values of α, both PEG combinations at 16.7 mg/mL, the highest concentration studied by Smolarsky [10], produced a diffusive exponent value approximately equal to 1, $\alpha = 1$. This value is consistent with a system experiencing basic diffusion. However, once the concentration was increased to 25 mg/mL, both PEG length combinations exhibited diffusive exponents below 1, $\alpha < 1$. Just below 1, the average diffusive exponent for tracer particles in an aqueous solution of PEG 2000 and 8000 at a concentration of 25 mg/mL was 0.996 ± 0.002. Even lower than this, PEG lengths 200 and 20000 at the same 25 mg/mL concentration resulted in a diffusive exponent value of $\alpha = 0.966 \pm 0.015$. Finally, the lowest experimentally found value for tracer particle diffusive exponent, $\alpha = 0.82 \pm 0.02$, was found in an aqueous solution of PEG length 200 at a 40% volume concentration and length 20000 at 20 mg/mL. All of the measured diffusive exponents less than 1, $\alpha < 1$, are suggestive of anomalous diffusion of the tracer particles. More specifically these values correspond to tracer particles undergoing subdiffusion.

Diffusion Coefficient, A		
Sample Code	**Average A**	**Uncertainty in A**
1	0.967	0.006
2	1.0651	0.0014
3	0.73	0.08
4	0.889	0.009
5	0.187	0.012

Table 4: Experimentally determined average diffusion coefficients, A, for each of the five possible PEG concentrations and polymer chain length combinations in the aqueous solution. Individual data points that make up the average can be found in **Appendix 2 - 6**.

Similarly to the observed diffusive exponent trends, the diffusion coefficient A of tracer particles in an aqueous solution with mixed-length PEG decreased with an increase in PEG concentration. The diffusion coefficient A also decreases with an increase in the length difference between the combined PEG molecules. It is important to note that the aforementioned in section 8.1 discrepancy between the measured general diffusion coefficient, A, and the theoretical diffusion coefficient, D, does not negate the usefulness of A in describing tracer particle motion given its direct reliance on D.

9 Discussion: Tracer Diffusion and PEG

9.1 Summary of Results

An analysis of the motion of fluorescently dyed tracer particles in aqueous solutions with two different lengths of PEG (2000 & 8000 or 200 & 20000) at varying densities (16.7 mg/mL, 25 mg/mL, or PEG 200 at 40% volume and 20000 at 20 mg/mL) showed the slope of MSD over time to decrease with an increase in PEG concentration and increased length difference between the two included PEG polymer chain lengths. MSD values were plotted on a log-log graph against lag time and were used to calculate a diffusion coefficient, A, and diffusive exponent, α, for each sample recording. The diffusion coefficient, A, was found to decrease with both an increased PEG concentration and an increase in the length difference between the two included PEG polymer chain lengths. Similarly, the diffusive exponent, α, decreased with both an increase in PEG concentration and length difference between the two included PEG chain lengths. More explicitly, basic diffusion where $\alpha = 1$ was observed for both polymer chain length combinations, 2000 & 8000 and 200 & 20000, at 16.7 mg/mL. All other samples examined, at higher concentrations, exhibited anomalous subdiffusion where $\alpha < 1$. No samples showed superdiffusion where $1 < \alpha < 2$.

9.2 Interpretation of Results

The noted decrease in diffusion coefficient, A, with increased PEG concentration suggests that the diffusion coefficient depends on the crowdedness of a diffusive medium– i.e. an increasingly crowded medium, one with a higher concentration of PEG, results in a lower diffusion coefficient. This finding is comparable to that of Smolarsky's work with aqueous solutions containing just one polymer chain length of PEG [10]. In addition, the evident decrease in A with an increased difference between included PEG polymer chain lengths implies that the diffusion coefficent relies on the variation of particle sizes within a studied aqueous solution.

Differentiating from Smolarsky's findings using one polymer chain length of PEG, this study suggests that anomalous subdiffusion, $\alpha < 1$, is observable at high enough concentrations when two differing polymer chain lengths of PEG are mixed into the aqueous solution. The discernible decrease in the diffusive exponent α with an increase in PEG concentration suggests that the diffusive exponent relies on the crowdedness of the diffusive medium. This decrease may also be attributed to the corresponding increase in the difference

between included PEG polymer chain lengths. This suggests that the diffusive exponent additionally depends on the variation of particle sizes within the solution.

The experimental identification of anomalous diffusion in an artificial cytoplasm is an important finding in the work of properly replicating biological cytoplasm's crowdedness. Despite being a fraction of the concentration used in Sunol and Zia's theoretical work [1], these experimental findings support the use of PEG as an artificial replication for the crowdedness of biological cytoplasm.

Influential to the application of these findings, the polymer structure of PEG is similar to many types of lipids, and it is therefore likely that similar trends would occur with biomolecules in biological cytoplasm [10]. Moreover, in considering the impact of PEG chain lengths, it is notable that the monomer length of PEG is 0.35 nm [22]. Comparatively, the sizes of many intracellular proteins are on the order of nanometers [23]. The similarity in size range of PEG with many biomolecules suggest that the results of this experiment regarding size differences in mixed PEG polymer lengths are applicable to the passive diffusion within biological intracellular environments [10].

9.3 Sources of Error and Their Treatment

The greatest source of error within this study was the presence of ensemble drift. Discussed in section 3.1.2, ensemble drift refers to the collective slow movement towards something. While the slides used for tracer particle observation were sealed from the external environment, they were not entirely free of drift.

To combat the error introduced by ensemble drift, a TrackPy script initially used by Horowitz et al. (2019) [5] was used to subtract calculated rotational and translational drift from particle trajectories as discussed in section 5.2.2. In addition to the TrackPy drift subtraction, the inclusion of mineral oil in the sealed sample slides contributed slightly to the reduction of drift as the hydrophobic nature of oil helped to minimize evaporation of the aqueous solution in the sample.

Additionally impactful to the study of tracer particle movement is the added noise in eMSD plots at longer time intervals. Measured eMSD values represent the averages of all iMSD for each tracer particle in a video. As particles move into and out of focus over time, as well as on and off the recorded section, particles are dropped and the resulting eMSD average is based on fewer particles. This noise impacts both eMSD values and the resulting measurements for the diffusion coefficient A and diffusive exponent α.

For every sample slide, three videos of approximately 500 frames each were taken. Given this long time interval, the impact of dropped particles may be more pronounced in this study than in Smolarsky's which analyzed videos of approximately 167 frames each [10]. To address this error, the standard deviation for α and A measurements for a single sealed sample slide was used as their uncertainty.

9.4 Dimensions of the General Diffusion Coefficient

Given the limitations of the power law used to calculate the general diffusion coefficient A and the diffusive exponent α, as in Eqn. 18, the general diffusion coefficient does not have set dimensions. Rather, its dimensions vary based on the value of the diffusive exponent α. In the specific case of basic diffusion where $\alpha = 1$, the dimensions of A may be identified as square meters per second [10]. For this study, the value of A remains dimensionless and it is instead noted that the value is determined given MSD is in units micrometre squared and time in seconds.

10 Future Research and Conclusion

10.1 Future Research

Given the discovered inability for the perfusion chamber to stick to the microscope slide within this drift-reducing chamber, future students may instead try to replicate Palacci's entire drift-reducing chamber manifold [2]. If successful, the replication of this device would allow for the study of self-propulsive Janus particles, particularly the effects of their coupling with inert tracer particles.

Applying the promising experimental findings of this study, a proper drift-reducing chamber may then be combined with multiple polymer chain lengths of PEG to produce a more accurate artificial model for an intracellular environment. Future studies may additionally examine higher concentrations of PEG to allow for greater variations in modeled cytoplasm.

Such a flexible artificial model of the cytoplasm would allow for greater future study of biomolecular motion and thus biological processes.

10.2 Conclusion

Tracer particle diffusion was measured in aqueous solutions containing various concentrations of two different PEG polymer chain lengths. In these samples, both the diffusion coefficient, A, and the diffusive exponent, α were found to decrease with both an increase in PEG concentration and an increase in the length difference between the two included PEG chain lengths. These findings suggest that the diffusion coefficient and diffusive exponent of tracer particles depend on both the medium's crowdedness and the variation of particle sizes within said medium.

Furthermore, the experimental findings of this work indicate that anomalous subdiffusion, $\alpha < 1$, is observable at high enough concentrations when two differing PEG polymer chain lengths are included in the aqueous solution. This important finding experimentally supports the theoretical work of Sunol and Zia [1] and aligns with the use of PEG for artificial replication of the crowdedness of biological cytoplasm.

In addition to the study of tracer particle diffusion, the feasibility of a perfusion-chamber based drift-reducing chamber was examined. Despite the optimization of such a chamber, in relation to agarose hydrogel

specifications and construction methods, it was found to be unsuitable due to its inability to maintain a seal when fluid was introduced to the system. Regardless of the failure to construct this easily reproducable drift-reduction chamber, the tracer particle findings of this study have extremely exciting implications for the artificial cells project and general work towards the creation of an artificial cell.

Bibliography

[1] Alp M. Sunol and Roseanna N. Zia. Confined brownian suspensions: Equilibrium diffusion, thermodynamics, and rheology. *Journal of Rheology*, 67(2):433–460, 2023.

[2] Jérémie Palacci. *Manipulation of colloids by osmotic forces*. PhD thesis, 2010.

[3] K Luby-Phelps, P E Castle, D L Taylor, and F Lanni. Hindered diffusion of inert tracer particles in the cytoplasm of mouse 3t3 cells. *Proceedings of the National Academy of Sciences*, 84(14):4910–4913, 1987.

[4] Donald L. Ermak and J. A. McCammon. Brownian dynamics with hydrodynamic interactions. *The Journal of Chemical Physics*, 69(4):1352–1360, 1978.

[5] Viva R Horowitz, Zachary C Chambers, Irep Gozen, Thomas G Dimiduk, and Vinothan N Manoharan. Active colloidal particles in emulsion droplets: A model system for the cytoplasm. *The European Physical Journal Special Topics*, 227(17):2413–2424, 2019.

[6] W. van Megen and S. M. Underwood. Tracer diffusion in concentrated colloidal dispersions. iii. mean squared displacements and self-diffusion coefficients. *The Journal of Chemical Physics*, 91(1):552–559, 1989.

[7] K. W. Kehr, K. Binder, and S. M. Reulein. Mobility, interdiffusion, and tracer diffusion in lattice-gas models of two-component alloys. *Physical Review B*, 39(8):4891–4910, 1989.

[8] Kyriacos C. Leptos, Jeffrey S. Guasto, J. P. Gollub, Adriana I. Pesci, and Raymond E. Goldstein. Dynamics of enhanced tracer diffusion in suspensions of swimming eukaryotic microorganisms. *Physical Review Letters*, 103(19), 2009.

[9] Jonathan R. Howse, Richard A. Jones, Anthony J. Ryan, Tim Gough, Reza Vafabakhsh, and Ramin Golestanian. Self-motile colloidal particles: From directed propulsion to random walk. *Physical Review Letters*, 99(4), 2007.

[10] Ryan Smolarsky. Diffusion and drift reduction in artificial cells, 2022.

[11] Poly(ethylene glycol). Chemsrc. `https://www.chemsrc.com/en/cas/25322-68-3_766012.html`.

[12] Coverwell™ perfusion chambers. Grace Bio-Labs, May 2018. `https://gracebio.com/products/imaging-microscopy/coverwell-perfusion-chambers-imaging/`.

[13] Daniel V. Schroeder. *An introduction to thermal physics*. Oxford University Press, 2021.

[14] Albert Einstein. *Investigations on the theory of, the Brownian movement*. Dover, 1956. ed: Fürth, R., Translator: Cowper, A. D.

[15] Daniel S. Banks and Cécile Fradin. Anomalous diffusion of proteins due to molecular crowding. *Biophysical Journal*, 89(5):2960–2971, 2005.

[16] Xu Zheng, Borge ten Hagen, Andreas Kaiser, Meiling Wu, Haihang Cui, Zhanhua Silber-Li, and Hartmut Löwen. Non-gaussian statistics for the motion of self-propelled janus particles: Experiment versus theory. *Physical Review E*, 88(3), 2013.

[17] Sara Ryding. Fluorescence microscopy vs. light microscopy, Nov 2018. `https://www.news-medical.net/life-sciences/Fluorescence-Microscopy-vs-Light-Microscopy.aspx`.

[18] Introduction to trackpy. Introduction to Trackpy - trackpy 0.6.1 documentation. `http://soft-matter.github.io/trackpy/v0.6.1/introduction.html`.

[19] Justine J. Roberts, Audrey Earnshaw, Virginia L. Ferguson, and Stephanie J. Bryant. Comparative study of the viscoelastic mechanical behavior of agarose and poly(ethylene glycol) hydrogels. *Journal of Biomedical Materials Research Part B: Applied Biomaterials*, 99B(1):158–169, 2011.

[20] Abigail Plummer, Caroline Adkins, Andrej Košmrlj, and Sujit S. Datta. Obstructed swelling and fracture of hydrogels, 2023.

[21] Thibault Bertrand, Jorge Peixinho, Shomeek Mukhopadhyay, and Christopher W. MacMinn. Dynamics of swelling and drying in a spherical gel. *Physical Review Applied*, 6(6), 2016.

[22] Devika B Chithrani. Polyethylene glycol density and length affects nanoparticle uptake by cancer cells. *Journal of Nanomedicine Research*, 1(1), 2014.

[23] Peter Schuck, Matthew A. Perugini, Noreen R. Gonzales, Geoffrey J. Howlett, and Dieter Schubert. Size-distribution analysis of proteins by analytical ultracentrifugation: Strategies and application to model systems. *Biophysical Journal*, 82(2):1096–1111, 2002.

11 Appendix

Appendix 1. Experimentally determined height values of a flat-bottomed agarose hydrogel with height 2.0 mm over time in RO water. Hydrogel swelling was calculated by subtracting the previous height measurement from the current one.

Agarose Hydrogel Swelling: flat-bottomed 2.0 mm tall cylinder		
Time (min)	**Average Height (mm)**	**Hydrogel Swelling (mm)**
0	1.94	
5	2.06	0.12
10	2.14	0.08
15	2.14	0
20	2.15	0.01
25	2.15	0
30	2.15	0
35	2.16	0.01
40	2.16	0
45	2.15	-0.01
60	2.15	0
120	2.15	0
180	2.18	0.03

Appendix 2. Experimentally determined diffusive exponent α and diffusion coefficient A for tracer particles in an aqueous solution with PEG lengths 2000 and 8000 at 25 mg/mL concentration.

2000 & 8000 @ 25 mg/mL		
Video Number	α	A
1	0.993251065	0.890843689
2	0.9979482462	0.8973782553
3	0.9967480758	0.8788599191
Average Value	0.996	0.889
Uncertainty in Value	0.002	0.009

Appendix 3. Experimentally determined diffusive exponent α and diffusion coefficient A for tracer particles in an aqueous solution with PEG lengths 200 and 20000 at 25 mg/mL concentration.

200 & 20000 @ 25 mg/mL			
Slide Number	**Video Number**	α	A
1	1	0.9840619718	0.8265540812
1	2	0.9752003473	0.8130156377
1	3	0.9917471397	0.8281362666
2	1	0.9355865539	0.6728731943
2	2	0.9745285032	0.7003261139
2	3	0.9562213082	0.6349561693
3	1	0.990313616	0.710672297
3	2	0.9435834189	0.6914055242
3	3	0.9441654839	0.6655515749
	Average Value	0.966	0.73
	Uncertainty in Value	0.015	0.08

Appendix 4. Experimentally determined diffusive exponent α and diffusion coefficient A for tracer particles in an aqueous solution with PEG lengths 2000 and 8000 at 16.7 mg/mL concentration.

2000 & 8000 @ 16.7 mg/mL		
Video Number	α	A
1	1.001648152	1.063659216
2	0.998475229	1.065304071
3	1.015501761	1.066457721
Average Value	1.005	1.0651
Uncertainty in Value	0.009	0.0014

Appendix 5. Experimentally determined diffusive exponent α and diffusion coefficient A for tracer particles in an aqueous solution with PEG lengths 200 and 20000 at 16.7 mg/mL concentration.

200 & 20000 @ 16.7 mg/mL		
Video Number	α	A
1	1.004550208	0.9621103064
2	0.9973505227	0.9644265109
3	1.009645521	0.9737807798
Average Value	1.004	0.967
Uncertainty in Value	0.006	0.006

Appendix 6. Experimentally determined diffusive exponent α and diffusion coefficient A for tracer particles in an aqueous solution with PEG length 200 at 40% volume and length 20000 at 20 mg/mL concentration.

200 @ 40% volume & 20000 @ 20 mg/mL		
Video Number	α	A
1	0.8186988726	0.1914903027
2	0.8409767284	0.1741319063
3	0.7921199043	0.1964659673
Average Value	0.82	0.187
Uncertainty in Value	0.02	0.012